Alunite–Jarosite Crystallography, Thermodynamics, and Geochronology

Article *in* Reviews in Mineralogy and Geochemistry · January 2000

DOI: 10.2138/rmg.2000.40.9

3 authors, including:

Roger E. Stoffregen

21 PUBLICATIONS **1,297** CITATIONS

SEE PROFILE

Charles N Alpers

United States Geological Survey

168 PUBLICATIONS **5,426** CITATIONS

SEE PROFILE

9

Alunite-Jarosite Crystallography, Thermodynamics, and Geochronology

R. E. Stoffregen
AWK Consulting Engineers, Inc.
1611 Monroeville Avenue,
Turtle Creek, Pennsylvania 15145

C. N. Alpers
U.S. Geological Survey
Water Resources Division,
6000 J Street Sacramento, California 95819

J. L. Jambor
Leslie Research and Consulting
316 Rosehill Wynd
Tsawwassen, British Columbia, Canada V4M 3L9

The alunite supergroup consists of more than 40 mineral species that have in common the general formula $DG_3(TO_4)_2(OH,H_2O)_6$. The *D* sites are occupied by monovalent (e.g. K, Na, NH_4, Ag, Tl, H_3O), divalent (e.g. Ca, Sr, Ba, Pb), trivalent (e.g. Bi, REE) or more rarely quadrivalent (Th) ions; *G* is Al or Fe^{3+} or rarely Ga or V; *T* is S^{6+}, As^{5+}, or P^{5+}, and may include subordinate amounts of Cr^{6+} or Si^{4+}. Many of the minerals in this supergroup are exotic, having been described from relatively few localities worldwide, generally in association with ore deposits. Rarely are end-member compositions attained in these natural occurrences, and extensive solid solution is typical for one or more of the *D*, *G*, and *T* sites. In this chapter, the two solid-solution series considered in detail are alunite-natroalunite [$KAl_3(SO_4)_2(OH)_6 - NaAl_3(SO_4)_2(OH)_6$] and jarosite-natrojarosite [$KFe_3(SO_4)_2(OH)_6 - NaFe_3(SO_4)_2(OH)_6$]. These minerals are by far the most abundant naturally occurring species of the alunite supergroup.

Minerals with the generalized formula cited above can be variously grouped, but the simplest initial subdivision is on the basis of Fe > Al versus Al > Fe. Further subdivision is generally made on the basis of the predominant cation within the two TO_4 sites. Thus, within the supergroup, the alunite group consists of minerals in which both of the *T* sites are occupied by sulfur. This leads to a total negative charge of four on the TO_4 sites. In the ideal formulas of some members of the supergroup [e.g. woodhouseite, $CaAl_3(PO_4)(SO_4)(OH)_6$], half of the *T* sites are occupied by sulfur, and the other half by arsenic or phosphorus, which produces a total negative charge of five on the TO_4 sites. In still other end-members of the supergroup [e.g. crandallite, $CaAl_3(PO_4)_2(OH)_5(H_2O)$, and arsenocrandallite, $CaAl_3(AsO_4)_2(OH)_5(H_2O)$], both of the *T* sites are occupied solely by phosphorus or arsenic, thus producing a total negative charge of six on the TO_4 sites (see Table 1 of Dutrizac and Jambor, this volume). In this chapter, however, the primary concern is with those minerals for which TO_4 is represented by SO_4^{2-} (Table 1).

Precipitates with compositions near those of the end-members in the system alunite-natroalunite and jarosite-natrojarosite are readily prepared using sulfate salts. The products, however, almost invariably have a slight to appreciable deficiency in G^{3+}, and have an apparent non-stoichiometry for *D*. The latter may reflect incorporation a H_3O^+, a

1529-6466/00/0040-0009$05.00 DOI: 10.2138/rmg.2000.40.9

Table 1. Minerals of the alunite group.

Alunite Subgroup		*Jarosite Subgroup*	
alunite	$KAl_3(SO_4)_2(OH)_6$	jarosite	$KFe_3(SO_4)_2(OH)_6$
natroalunite	$NaAl_3(SO_4)_2(OH)_6$	natrojarosite	$NaFe_3(SO_4)_2(OH)_6$
ammonioalunite	$(NH)_4Al_3(SO_4)_2(OH)_6$	ammoniojarosite	$(NH_4)Fe_3(SO_4)_2(OH)_6$
schlossmacherite	$(H_3O,Ca)Al_3(SO_4)_2(OH,H_2O)_6$	hydronium jarosite	$(H_3O)Fe_3(SO_4)_2(OH)_6$
—		argentojarosite	$AgFe_3(SO_4)_2(OH)_6$
—		dorallcharite	$TlFe_3(SO_4)_2(OH)_6$
osarizawaite	$Pb(Al,Cu)_3(SO4)_2(OH,H_2O)_6$	beaverite	$Pb(Fe,Cu)_3(SO_4)_2(OH,H_2O)_6$
—		plumbojarosite*	$PbFe_6(SO_4)_4(OH)_{12}$
minamite*	$(Na,Ca)_2Al_6(SO_4)_4(OH,H_2O)_{12}$	—	
huangite*	$CaAl_6(SO_4)_4(OH)_{12}$	—	
walthierite	$BaAl_6(SO_4)_4(OH)_{12}$	—	

**c* axis is ~34 Å, which is double that of other members

solid solution that is difficult to prove because H_3O^+ cannot be determined directly by wet-chemistry or microprobe methods. Nevertheless, the existence of two minerals in the alunite supergroup is dependent solely on their *D*-site predominance of H_3O^+, namely, hydronium jarosite [$(H_3O)Fe_3(SO_4)_2(OH)_6$] and schlossmacherite [$(H_3O,Ca)Al_3(SO_4)_2(OH,H_2O)_6$].

This chapter is organized into four sections. In the first section, crystallographic data for alunite-natroalunite and jarosite-natrojarosite are presented and discussed. The second section describes available thermodynamic data for these two solid-solution series, in terms of properties of the end-members and mixing properties for intermediate compositions. The third section discusses the geochemistry and occurrences of alunite and jarosite, and the last section summarizes the published literature on the use of alunite and jarosite in geochronology.

CRYSTALLOGRAPHIC DATA

The crystal structures of minerals within the alunite supergroup were first determined by Hendricks (1937), who reported data for alunite, jarosite, and plumbojarosite. Structure studies of numerous additional minerals within the supergroup have since been determined; although there are several exceptions, most of the minerals have trigonal symmetry, space group $R\bar{3}m$, and unit-cell parameters of a = ~7, c = ~7Å. Even among the exceptions, the minerals are strongly pseudotrigonal, and the basic topology of the structure remains the same regardless of chemical composition.

The basic structural motif of the supergroup consists of TO_4 tetrahedra and variably distorted octahedra of $G(O,OH)_6$. The latter corner-share hydroxyl ions, and two oxygen ions from two TO_4 tetrahedra, to form sheets parallel to the (001) plane, thereby forming a sequence that is perpendicular to the *c* axis. This arrangement is illustrated in Figure 1, a simplified representation of the alunite structure, and in Figure 2, a more detailed representation of the jarosite structure. Substitutions in *G* mainly affect the *a* dimension, and *a* increases as Fe-for-Al substitution increases. The TO_4 tetrahedra, which are aligned along [001], occur as two crystallographically independent sets within a layer; one set of TO_4 points upward along *c*, and this set alternates with another pointing downward. The oxygen and hydroxyl form a polyhedron amidst which is the *D* cation, sandwiched between the sheets of $G(O,OH)_6$ octahedra. Thus, if TO_4 sites are entirely occupied by

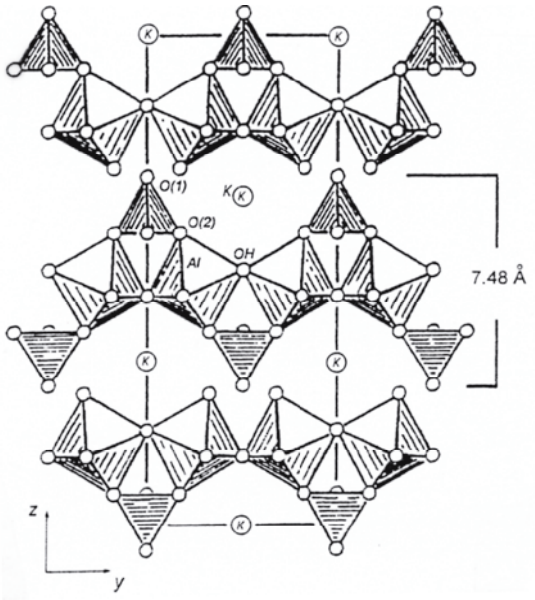

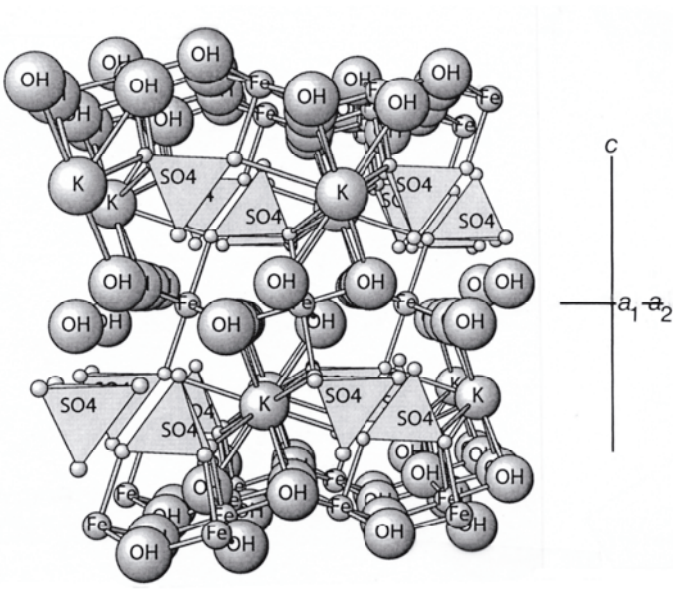

Figure 1 (left). The structure of alunite, viewed parallel to the *a* axis. (Slightly modified from Menchetti and Sabelli 1976).

Figure 2 (right). The structure of jarosite, viewed parallel to the *a* axis. (Illustration courtesy of Eric Dowty).

SO_4, variations in the length of *c* are mainly influenced by the size of the *D* cation. In the natroalunite–alunite and natrojarosite–jarosite series, therefore, as compositions approach those of alunite and jarosite the length of the *c* parameter increases as a consequence of the larger ionic radius of K versus Na. A corresponding increase in *a* does not occur because the expected expansion is instead accommodated by a closer fitting of the rough surfaces of the sheet-like layers of octahedra (Menchetti and Sabelli 1976, Okada et al. 1982).

Symmetry changes within the supergroup arise mainly because of ordering of the TO_4 tetrahedra, or because of ordering or distortion effects within *D* sites. Ordering of TO_4 reduces the symmetry, generally from $R\bar{3}m$ to $R3m$. As was discussed by Szymanski (1985), however, the space group of alunite-jarosite minerals should be assumed to be $R\bar{3}m$ unless structure data prove otherwise. Ordering of *D*-site cations can lead to a doubling of the length of *c*, an effect that is especially evident in alunite-group minerals in which *D* is occupied by a divalent element (Table 1). In plumbojarosite, for example, half of the *D* sites are vacant because of the need to maintain electroneutrality. Ordering of the Pb^{2+} and the vacancies produces a supercell with $c = 33–34$ Å.

Non-stoichiometry in both *D* and *G* is common, particularly in synthetic samples and in minerals in which *D* is occupied by a combination of monovalent and divalent elements. Calculation of formulas on the basis of $TO_4 = 2$ is the preferred approach because, whereas deficiencies in *D* and *G* occupancy may be tolerable, it is not possible to maintain a coherent structure with vacancies in TO_4.

The compositions of all of the minerals within the alunite supergroup are characterized by a predominance of SO_4, AsO_4, or PO_4. Extensive solid solution among these, well beyond that known at the time of Palache et al. (1951), is prevalent in many of the phosphate and arsenate members. Although the TO_4 groups provide well defined boundaries for a ternary system of nomenclature (Jambor 1999), the boundaries currently are set at 25 and 75 mol % (Scott 1987). For example, the composition of beudantite,

which is generally assigned the formula $PbFe_3(AsO_4)(SO_4)(OH,H_2O)_6$, extends from $PbFe_3[(SO_4)_{0.75}(AsO_4)_{0.25}](OH,H_2O)_6$ to $PbFe_3[(SO_4)_{0.25}(AsO_4)_{0.75}](OH,H_2O)_6$, wherein OH is converted to H_2O, as necessary, to achieve charge balance. Compositions with the molar site occupancy of >0.75 total SO_4 on the *T* site apply to plumbojarosite, and those with AsO_4 > 0.75 are segnitite. The consequence is that, within each compositional triangle with AsO_4, PO_4, and SO_4 at the apices, five mineral names are permitted rather than three more rigorously applicable to a ternary system.

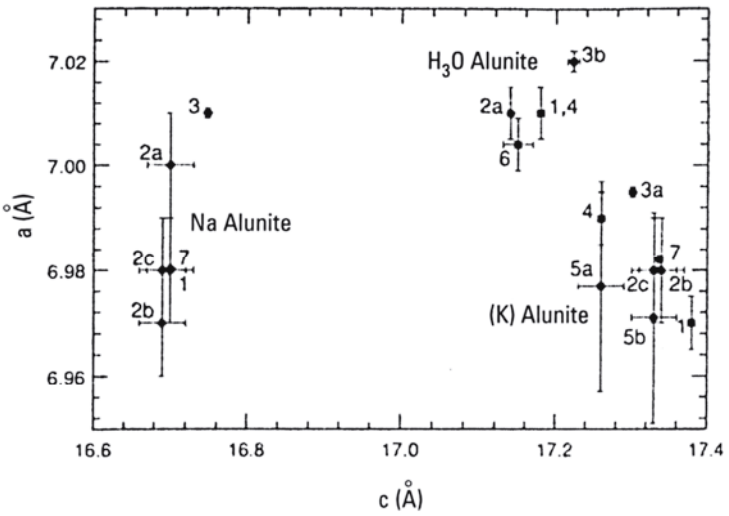

Figure 3. Variations in the unit-cell dimensions of alunite, natroalunite, and schlossmacherite (hydronium alunite). Sources of data: 1 = Kashkai (1969); 2 = Parker (1962): 2a = synthetic alunite and natroalunite (not heated, contain hydronium), 2b = synthetic alunite and natroalunite (heated, contain no hydronium), 2c = natural; 3 = Menchetti and Sabelli (1976): 3a = single crystal, 3b = powder; 4 = Kubisz (1964, 1970); 5 = Brophy and Sheridan (1965): 5a = synthetic, 5b = natural; 6 = Ripmeester et al. (1986); 7 = Stoffregen and Alpers (1992). Modified from Alpers et al. (1992).

Unit-cell parameters

Alunite. Stoffregen and Alpers (1992) provided a review of unit-cell parameters for synthetic and natural alunite. Published unit-cell dimensions for "end-member" alunite, natroalunite, and hydronium alunite are shown in Figure 3. The large range in *a* and *c* for each end-member is probably the result of non-hydroxyl water (most likely as hydronium ion) in some samples. For example, Menchetti and Sabelli (1976) reported a *c* value for alunite which is about 0.1 Å lower than most other published values. On the basis of their description of the synthesis method used, this lower value almost certainly reflects the presence of non-hydroxyl water in their sample. Many other studies do not provide on information on the water content of the samples (e.g. Wang et al. 1965), and as such the results cannot be assumed to be representative of stoichiometric alunite or natroalunite.

Published data for unit-cell dimensions of alunite can be compared with results obtained for synthetic samples by Stoffregen and Alpers (1992; Table 2, Fig. 3). Unit-cell dimensions for the end-member alunite samples synthesized at 250 and 450°C agree within 2σ for *c* and *a*, whereas the sample obtained at 150°C has significantly higher *a* and lower *c* and cell volume (V). These results are similar to data from Parker (1962) for alunite synthesized at 100°C, for which *c* increased and *a* decreased after heating in air for one hour at 300°C. Parker attributed this shift in unit-cell dimensions to the loss of non-hydroxyl water (hydronium) during heating. This loss is confirmed by a decrease in water content from 128% of the amount predicted for stoichiometric alunite in the 150°C sample to about 105% of this amount in the other two synthetic alunite samples (Table 2).

Natroalunite. Unit-cell values for various samples of natroalunite are also shown in Figure 3. Table 2 indicates that natroalunite prepared at 150°C has a significantly larger value of *a* than those of the 250 and 450°C samples and also contains the most water of the three (Stoffregen and Alpers 1992).

Also given in Table 2 are unit-cell data for synthetic schlossmacherite (hydronium

Table 2. Unit-cell parameters for synthetic alunite-group minerals (from Stoffregen and Alpers 1992).

	***a*, Å**	***c*, Å**	***V*, Å^3**	**Excess Water** (% of stoich.)
Alunite (150°C)	7.000(2)	17.180(7)	729.1(4)	128.2
Alunite (250°C)	6.9831(5)	17.334(2)	732.03(9)	103.9
Alunite (450°C)	6.981(1)	17.331(4)	731.5(2)	105.5
Natroalunite (150°C)	6.9990(8)	16.690(3)	708.0(2)	119.6
Natroalunite (250°C)	6.9823(5)	16.700(2)	705.1(1)	113.0
Natroalunite (450°C)	6.9786(7)	16.696(3)	704.2(2)	99.1
Schlossmacherite	7.005(2)	17.114(7)	727.2(4)	n.d.
Jarosite (95°C)	7.310(1)	17.042(3)	788.8(2)	n.d.
Jarosite (200°C)	7.300(1)	17.216(4)	794.6(2)	n.d.
Natrojarosite (98°C)	7.336(2)	16.621(5)	774.7(3)	n.d.
Natrojarosite (200°C)	7.316(1)	16.590(3)	768.9(2)	n.d.

*Excess water computed as water content of samples divided by water content of stoichiometric end-member; n.d, not determined

alunite) prepared following the method of Ripmeester et al. (1986). For hydronium alunite, *c* is intermediate between those of alunite and natroalunite, but *a* is 7.005(2) Å. The value for *a* is similar to those of alunite and natroalunite samples prepared at 150°C, but is significantly larger than the 6.978-6.983 Å range obtained for the alunite and natroalunite samples prepared at 250 and 450°C. These results suggest that the presence of significant non-hydroxyl water in alunite can be recognized by an anomalously large value of *a*, which should be apparent regardless of the Na content of the sample.

Jarosite. Values of *a* and *c* for jarosite, natrojarosite, and hydronium jarosite are plotted in Figure 4. The *c* dimension for jarosite is slightly lower than that for alunite (17.24 versus 17.32 Å), and the *a* value for jarosite is significantly larger, at between 7.28 and 7.34 Å versus about 6.98 Å for alunite. As with alunite, the range of unit-cell values reported for jarosite seems to be due in large part to variations in the hydronium content. This relationship is particularly evident in the two samples from Stoffregen (unpublished data): the sample synthesized at 95°C had *a* =7.310(1) and *c* =17.042(3) Å, whereas the same sample heated to 200°C had *a* =7.300(1) and *c* =17.216(4) Å (Table 2, Fig. 4).

Natrojarosite. Unit-cell data for natrojarosite (Fig. 4) show values of *a* in the range of 7.29 to 7.33 Å, and *c* in the range of 16.5 to 16.7 Å. As with jarosite, the trend is for higher values of *a* to be associated with samples known or inferred to have an appreciable hydronium content. However, as discussed later, there also seems to be a slight increase in *a* that is related to the Na content.

THERMODYNAMIC DATA

Alunite and natroalunite

Overviewof stability relations. The stability relations of alunite with silicate minerals in the system K–Al–Si–SO_4 are defined by the following reactions to form muscovite (Eqn. 1), kaolinite (Eqn. 2) (or pyrophyllite), and K-feldspar (Eqn. 3)

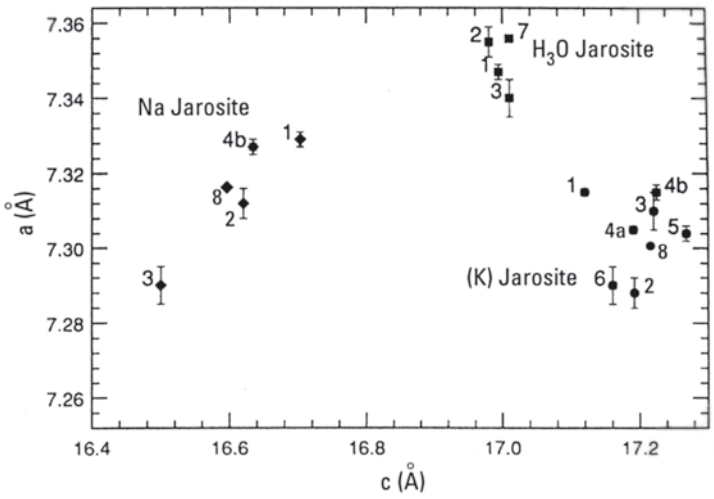

Figure 4. Variations in the unit-cell dimensions of jarosite, natro-jarosite, and hydronium jarosite. Sources of data: 1 = Dutrizac and Kaiman (1976; JCPDS card 301203); 2 = Brophy and Sheridan (1965); 3 = Kubisz (1970); 4 = Menchetti and Sabelli (1976): 4a = powder, 4b = single crystal; 5 = Kato and Miúra (1977; JCPDS card 22-827); 6 = JCPDS card 22-827; 7 =JCPDS card 31-650; 8 = synthetic jarosite and natrojarosite (250°C), Stoffregen, unpublished data (see Fig. 12). Modified from Alpers et al. (1992).

(Hemley et al. 1969):

$$KAl_3(SO_4)_2(OH)_{6(s)} + 3\ SiO_{2(s)} \Leftrightarrow KAl_3Si_3O_{10}(OH)_{2(s)} + 2\ SO_4^{2-}{}_{(aq)} + 4\ H^+_{(aq)} \quad (1)$$

$$2\ KAl_3(SO_4)_2(OH)_{6(s)} + 6\ SiO_{2(s)} + 3\ H_2O \Leftrightarrow 3\ Al_2Si2_3O_5(OH)_{4(s)} + 4\ SO_4^{2-}{}_{(aq)} + 6\ H^+_{(aq)} + 2\ K^+_{(aq)} \quad (2)$$

and

$$KAl_3(SO_4)_2(OH)_{6(s)} + 9\ SiO_{2(s)} + 2\ K^+_{(aq)} \Leftrightarrow 3\ KAl_3Si_3O_{8\ (s)} + 2SO_4^{2-}{}_{(aq)} + 6\ H^+_{(aq)} \quad (3)$$

These reactions are generally represented in $\log(a^2_{H^+}a_{SO_4^{2-}}) - \log(a^2_{K^+}a_{SO_4^{2-}})$ activity space (e.g. Hemley 1969, Stoffregen 1987) as illustrated in Figure 5. The congruent reaction for alunite dissolution

$$KAl_3(SO_4)_2(OH)_{6(s)} + 6\ H^+_{(aq)} \Leftrightarrow 3\ Al^{3+} + K^+_{(aq)} + 2\ SO_4^{2-}{}_{(aq)} + 6\ H_2O_{(1)} \quad (4)$$

can also be presented on this type of diagram for a specified value of $\log(a^2_{Al^{3+}}a^3_{SO_4^{2-}})$ (Fig. 5). This reaction limits alunite stability at high H_2SO_4 concentrations.

In the absence of silica, the stability of alunite is defined by the alunite-böhmite reaction

$$KAl_3(SO_4)_2(OH)_{6(s)} \Leftrightarrow 3\ AlO(OH)_{(böhmite)} + K^+_{(aq)} + 2\ SO_4^{2-}{}_{(aq)} + 3\ H^+_{(aq)} \quad (5)$$

or the similar alunite-to-corundum reaction (Stoffregen and Cygan 1990). These reaction boundaries parallel the kaolinite-alunite reaction in Figure 5.

Data on the stability of alunite relative to silicate minerals have been obtained by Hemley et al. (1969). Experimental results at 200, 300, and 380°C from that paper are presented in Figure 6. As is discussed later, the assemblages alunite + kaolinite and alunite + kaolinite + muscovite (or illite) are common as part of the advanced argillic alteration. The invariant point for the assemblage alunite + muscovite + kaolinite (or pyrophyllite) + quartz in terms of total molal H_2SO_4 and K_2SO_4, respectively, was reported at 0.002*m* and 0.03*m* at 200°C; 0.012*m* and 0.013*m* at 300°C; and 0.02*m* and 0.016*m* at 380°C. In contrast, the natural assemblages alunite + K-feldspar and alunite + K-feldspar + muscovite have not been reported. As noted by Hemley et al. (1969), this apparent absence suggests that the elevated K_2SO_4 concentrations required to stabilize such assemblages (Fig. 6) are rarely, if ever, obtained in nature.

The congruent reaction for alunite dissolution (Eqn. 4) has been used to evaluate the thermodynamic properties of alunite on the basis of its equilibrium relations with an aqueous phase in modern lake and hot-spring environments. Reaction (4) is also

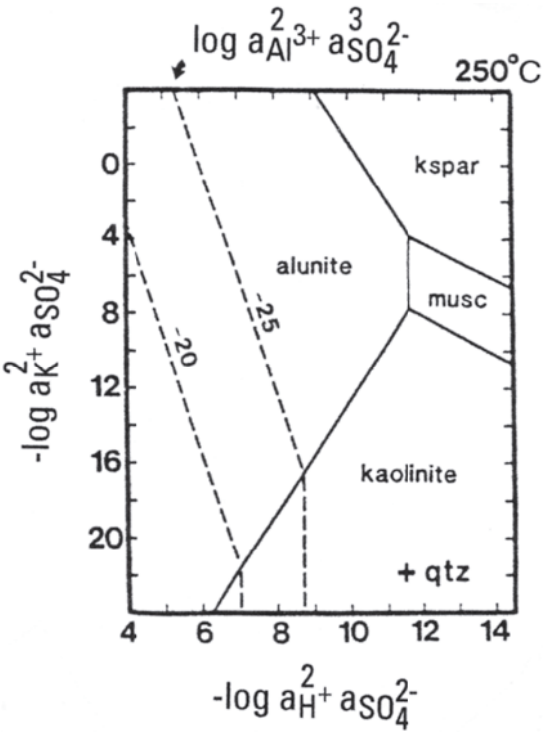

Figure 5. Alunite stability relations with silicate minerals at 250°C. Modified from Stoffregen (1987).

applicable to the interpretation of advanced log argillic alteration, which is limited by the formation of an intensely leached, predominantly quartz-only assemblage. This type of alteration is typified by the so-called vuggy silica rock. The congruent reaction for alunite dissolution has not been studied experimentally at elevated temperature.

The alunite-böhmite and alunite-corundum reactions have not been studied experimentally, except indirectly in alkali-exchange experiments conducted by Stoffregen and Cygan (1990). In their experiments at 450°C, alunite reacted with 0.5*m* $(K,Na)_2SO_4$ – 0.3*m* H_2SO_4 solutions to form corundum. When the initial H_2SO_4 concentration was 1.0 *m*, alunite reacted to form an Al-sulfate compound that is of uncertain stoichiometry and that has not been reported in nature. The silica-free system may be relevant to certain occurrences of alunite in Al-rich intermediate-grade metamorphic as discussed below.

End-member thermodynamic data. Kelley et al. (1946) obtained heat-capacity data and an enthalpy of formation for a sample of Marysvale alunite and for a synthetic alunite. Subsequent work on the stability relations of alunite (e.g. Hemley et al. 1969, Helgeson et al. 1978) has generally been based on the data for the synthetic sample, presumably because of the impurities reported by Kelley et al. (1946) in the Marysvale

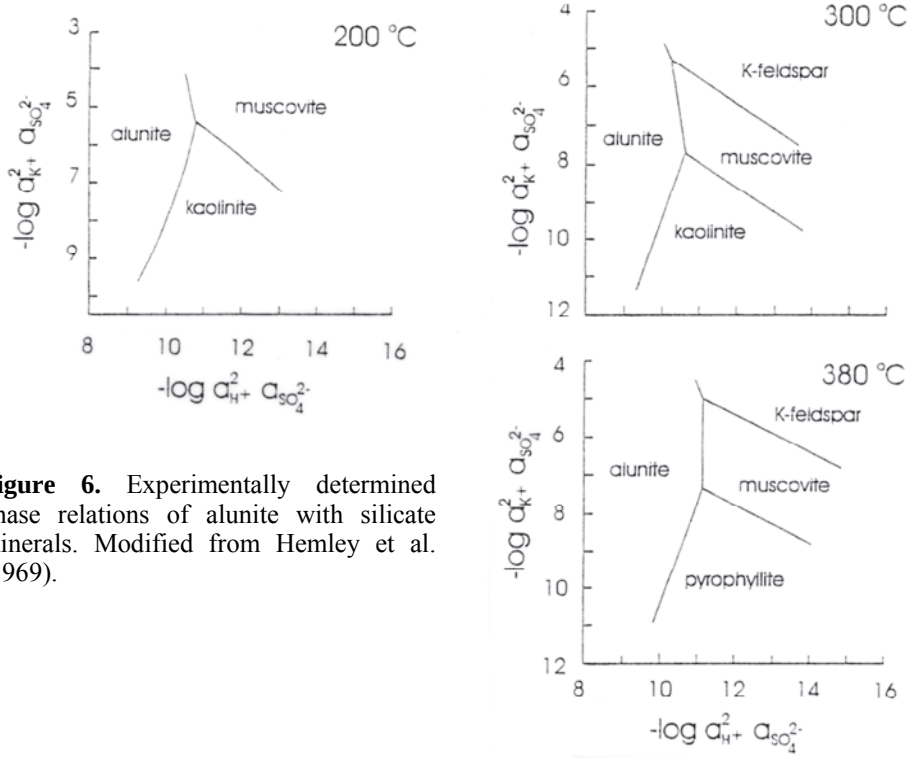

Figure 6. Experimentally determined phase relations of alunite with silicate minerals. Modified from Hemley et al. (1969).

alunite. As discussed above, many samples of synthetic alunite described in the literature seem to be non-stoichiometric because of the presence of hydronium. However, the 250°C synthesis temperature used by Kelley et al. (1946) is high enough to minimize the incorporation of hydronium, and their analytical data show the alunite to be almost stoichiometric. The Kelly et al. (1946) thermodynamic values for the synthetic alunite are also the values recommended here (Table 3).

Table 3. Recommended thermodynamic data for alunite group end-members.

	Units	Alunite	Natroalunite	Jarosite	Natrojarosite
$\Delta H_{f,298\ K,\ 1\ bar}$	kJ mol^{-1}	– 5169.8[a]	– 5131.97[c]	– 3715.1[d]	– 3673.1[d]
$S_{298K,\ 1\ bar}$	J mol^{-1}(K°)$^{-1}$	328.0[a]	321.08[c]	388.9[d]	382.4[d]
$\Delta G_{f,298\ K,\ 1\ bar}$	kJ mol^{-1}	– 4659.3[a]	– 4622.40[c]	– 3309.8[e]	– 3256.7[f]
a	J mol^{-1}(K°)$^{-1}$	642.03[b]	641.5[c]	616.89[d]	616.39[d]
b ($\times 10^{3}$)	J mol^{-1}(K°)$^{-2}$	0[b]	– 7.87[c]	98.74[d]	91.21[d]
c ($\times 10^{-5}$)	J mol^{-1}(K°)$^{-1}$	– 229.91[b]	– 234.12[c]	– 199.6[d]	– 203.76[d]

[a] Kelley et al. (1946); [b] Kelley (1960); [c] Stoffregen and Cygan (1990); [d] Stoffregen (1993); [e] Baron and Palmer (1996); [f] Kashkai et al. (1975)

Other published determinations of the free energy of formation of alunite have been based on mineral–water equilibrium (Kashkai et al. 1975, Raymahashay 1969, Zotov 1967). These values are considered to be less reliable than the data from Kelly et al. (1946) because the alunite that was used in the determinations was almost certainly non-stoichiometeric.

We are not aware of any published values for the entropy, enthalpy, or heat capacity of natroalunite. Stoffregen and Cygan (1990) used Na-K exchange data for alunite-natroalunite, together with a heat-capacity estimate based on the method of Helgeson et al. (1978), to obtain thermodynamic data for natroalunite at 25°C (Table 3). In the absence of measured thermodynamic data on natroalunite, the values from Stoffregen and Cygan (1990) are recommended.

Jarosite and natrojarosite

Overview of stability relations. Unlike alunite, jarosite does not display equilibrium relations with silicate minerals. Instead, the principal reaction that limits its stability in nature is simply its conversion to iron oxide or oxyhydroxide minerals. At surficial conditions, conversion of jarosite to goethite occurs by the reaction

$$KFe_3(SO_4)_2(OH)_{6(s)} \Leftrightarrow 3\ FeO(OH)_{(goethite)} + K^+_{(aq)} + 2\ SO^{2-}_{4\ (aq)} + 3\ H^+_{(aq)} \quad (6)$$

although this reaction may be complicated by the formation of metastable phases such as schwertmannite [$Fe_8O_8(OH)_{8-2x}(SO_4)_x$] and ferrihydrite (~$Fe_5HO_8 \cdot 4H_2O$) (Nordstrom and Alpers 1999, Bigham and Nordstrom, this volume). At temperatures above the goethite-to-hematite transition, which occurs at about 100°C for phases of equal surface area (Langmuir 1971), the incongruent dissolution reaction for jarosite becomes

$$KFe_3(SO_4)_2(OH)_{6(s)} \Leftrightarrow 1.5\ Fe_2O_{3(s)} + K^+_{(aq)} + 2\ SO^{2-}_{4\ (aq)} + 3\ H^+_{(aq)} + 1.5\ H_2O_{(1)} \quad (7)$$

The compound $Fe(SO_4)(OH)$ provides a second boundary to the jarosite field by the reaction

$$KFe_3(SO_4)_2(OH)_{6(s)} + 3\ H^+_{(aq)} + SO^{2-}_{4\ (aq)} \Leftrightarrow 3\ Fe(SO_4)(OH)_{(s)} + K^+_{(aq)} + 3\ H_2O_{(1)} \quad (8)$$

Although not reported in nature, $Fe(SO_4)(OH)$, which is the anhydrous equivalent of butlerite and related phases (see Bigham and Nordstrom, this volume), has been observed in several studies of the system H_2O–SO_3–Fe_2O_3 (Posnjak and Merwin 1922, Umetsu et al. 1977, Tozawa et al. 1983, Stoffregen 1993).

Reactions (7) and (8) can be used to define a field of jarosite stability in $\log(a^2_{H^+}a_{SO_4^{2-}}) - \log(a^2_{K^+}a_{SO_4^{2-}})$ space. This is illustrated in Figure 7, which indicates that jarosite should occur at $\log(a^2_{H^+}a_{SO_4^{2-}})$ values intermediate between those required to produce hematite and $Fe(SO_4)(OH)^4$ a given value of $\log(a^2_{K^+}a_{SO_4^{2-}})$ Figure 7 also implies that, at a given temperature and concentration of dissolved ferric iron, there is a minimum value of $\log(a^2_{K^+}a_{SO_4^{2-}})$ necessary for jarosite stability. This minimum is the jarosite-hematite-$Fe(SO_4)(OH)^4$ triple point. The stability limit for jarosite is reached when this triple point occurs at $\log(a^2_{K^+}a_{SO_4^{2-}})$ equal to the saturation value for potassium sulfate.

Also shown in Figure 7 are contours for the activity product $\log(a^2_{Fe^{3+}}a_{SO_4^{2-}})$ in equilibrium with each of the solid phases. These contours are based on the congruent dissolution reactions

$$KFe_3(SO_4)_2(OH)_{6(s)} + 6H^+_{(aq)} \Leftrightarrow K^+_{(aq)} + 2\,SO_4^{2-}{}_{(aq)} + 3Fe^{3+}_{(aq)} + 6H_2O_{(1)} \quad (9)$$

$$Fe_2O_{3(s)} + 6H^+_{(aq)} \Leftrightarrow 2Fe^{3+}_{(aq)} + 3H_2O_{(1)} \quad (10)$$

and

$$Fe(SO_4)(OH)_{(s)} + H^+_{(aq)} \Leftrightarrow Fe^{3+}_{(aq)} + SO_4^{2-}{}_{(aq)} + H_2O_{(1)} \quad (11)$$

The contours of $\log(a^2_{Fe^{3+}}a_{SO_4^{2-}})$ in Figure 7 imply that the amount of dissolved Fe in equilibrium with jarosite increases as $\log(a^2_{H^+}a_{SO_4^{2-}})$ and as $\log(a^2_{K^+}a_{SO_4^{2-}})$ decreases.

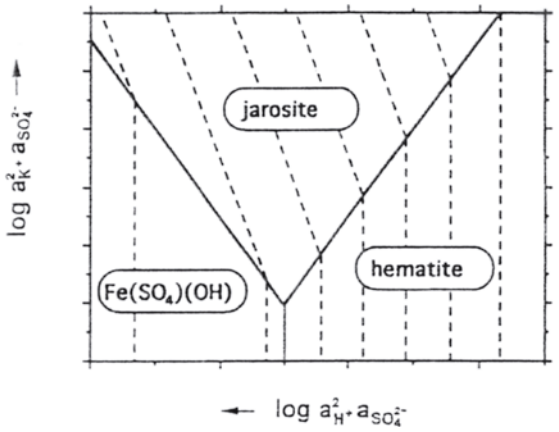

Figure 7. Schematic illustration of the stability relations of jarosite. Dashed lines represent contours of $\log(a^2_{Fe^{3+}}a^3_{SO4^{2-}})$, increasing to the left. Used by permission of Elsevier Science Ltd., from Stoffregen (1993), *Geochim Cosmochim Acta*, Vol. 57, Fig. 1, p. 2418.

The stability relations of jarosite have been studied primarily at surficial conditions, using Reaction (9). Numerous other studies on the phase relations in the system Fe–S–H_2O have been conducted, mainly for hydrometallurgical purposes (Dutrizac and Jambor, this volume). Stoffregen (1993) conducted experiments to identify the phase boundaries given by Reactions (7) and (8) at 150 to 250°C. These experiments indicated that a H_2SO_4 molality of 0.25 to 0.63 was required to stabilize jarosite over this temperature range (Fig. 8). Natrojarosite formed from hematite in experiments with H_2SO_4 of 0.79 *m* at 200°C but could not be produced from hematite at 250°C.

End-member thermodynamic data. The many determinations of the free energy of jarosite at surface conditions, based on assumed equilibrium between jarosite and a coexisting aqueous phase, have been summarized by Baron and Palmer (1996). The most reliable values are considered to be those of Alpers et al. (1989), Kashkai et al. (1975), Zotov et al. (1973), and Baron and Palmer (1996). The respective values for $\Delta G°_{f,298}$ are -3300.2±2.6; -3299.7±4; -3305.8±4; and -3309.8±1.7 kJ/mol. The recommended value is -3309.8±1.7 kJ/mol

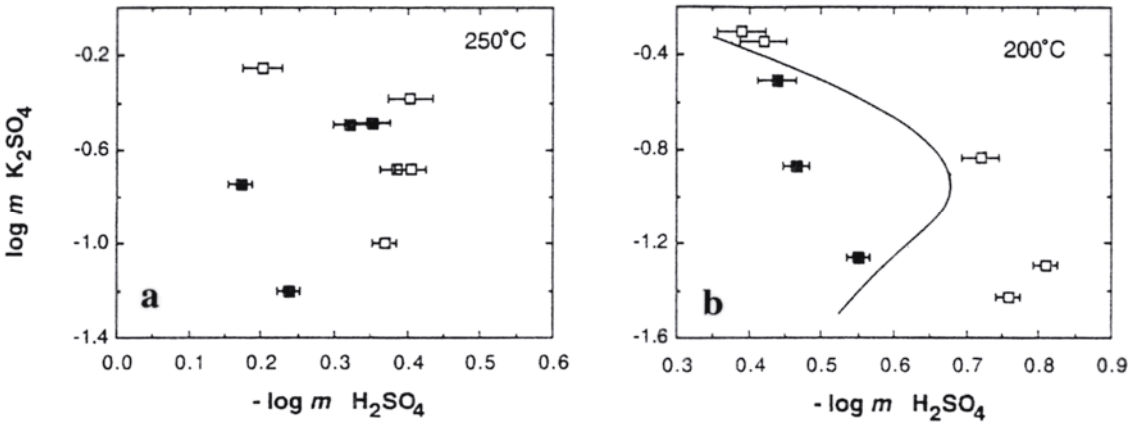

Figure 8. Experimentally determined jarosite-hematite boundary. Filled squares = hematite starting material, run product with both hematite and jarosite; open squares = jarosite starting material, run product with both hematite and jarosite. (a) 250°C; (b) 200°C. The solid line in (b) is the hematite-jarosite boundary computed with PHRQPITZ (see text). Error bars represent uncertainty in SO_4 and K measurements. Used by permission of Elsevier Science Ltd., from Stoffregen (1993), *Geochim Cosmochim Acta* Vol. 57, Fig. 2, p. 2420.

(Baron and Palmer 1996). Recommended enthalpy and entropy values for jarosite and natrojarosite are also included in Table 3. There are only a few published values for $\Delta G°_{f,298}$ of natrojarosite. The recommended value is -3256.7 kJ/mole reported by Kashkai et al. (1975).

For jarosite, Stoffregen (1993) reported a Gibbs free energy at 200°C of -3416.3 kJ/mole. On the basis of the experimental reversals shown in Figure 8, this value was computed using the program PHRQPITZ (Plummer et al. 1988) to model the aqueous phase. Because information on the temperature dependence of the H^+–HSO_4^-, K^+–HSO_4^- and Na^+–HSO_4^- interaction parameters was not available, all were assumed equal to the 25°C values in the computation. This assumption, and the high ionic strength of the coexisting aqueous phase (I = 0.33), introduce uncertainty into the free-energy value reported for jarosite. Nevertheless, the phase boundary predicted with PHRQPITZ is consistent with the reversals observed for Reaction (7).

No measured heat-capacity data are available for jarosite or natrojarosite. For both, Stoffregen (1993) presented values of the Meier-Kelley a, b, and c terms estimated from thermodynamic data on alunite, hematite, and corundum using the method of Helgeson et al. (1978). These values are listed in Table 3. The $\Delta G°_{f,298}$ of jarosite based on these values is -3328.4 kJ/mole, in poor agreement with the range of -3299.7 to -3310.4 kJ/mole discussed above. The discrepancy is thought to result from inaccuracies in the estimated thermodynamic parameters in Table 3, but it may also reflect errors in the determination of the aqueous activity coefficients, as noted above. Similarly, $\Delta G°_{f,298}$ for natrojarosite obtained from the data in Table 3 is 29 kJ more negative than the value reported by Kashkai et al. (1975).

Other minerals in the alunite-jarosite supergroup

The $\Delta G°$ values of synthetic goyazite $SrAl_3(PO_4)_2(OH,H_2O)_6$, arsenogoyazite $SrAl_3(AsO_4)_2(OH,H_2O)_6$, gorceixite $BaAl_3(PO_4)_2(OH,H_2O)_6$, arsenogorceixite $BaAl_3(AsO_4)_2(OH,H_2O)_6$, plumbogummite $PbAl_3(PO_4)_2OH,H_2O)_6$, florencite-(Ce) to -(Eu), and As analogs of the florencite minerals were reported by Schwab et al. (1993), who determined the equilibrium constants for dissolution reactions. Because of the low solubility of these minerals, at least one year was needed for each experiment, and there

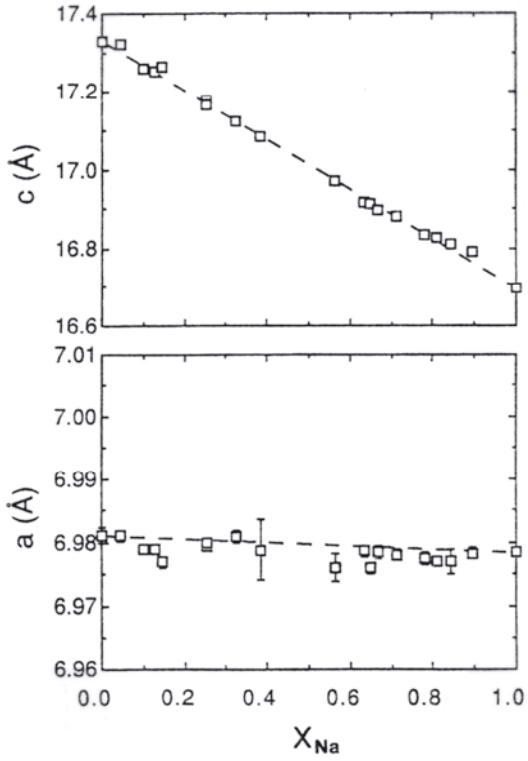

Figure 9. Unit-cell parameters of alunite as a function of Na mole fraction. From Stoffregen and Alpers (1992).

are significant uncertainties in the data because of the poor crystallinity and fine grain size of the precipitates. Nevertheless, Schwab et al. (1993) reported excellent agreement with independent estimates by Herold (1987) for the $\Delta G°_{f,298}$ of crandallite, although both studies used extrapolation from goyazite-crandallite solid solutions because pure crandallite could not be synthesized.

Mixing relations

Alunite-natroalunite. Stoffregen and Alpers (1992) presented data on unit-cell dimensions for 17 samples on the alunite–natroalunite binary. These samples were prepared in alunite–water Na-K exchange experiments at 450°C. The data are plotted as a function of composition in Figure 9, along with data for end-member alunite and natroalunite. The variation in *a* across this binary is approximately the same size as the average 2σ for *a* and is thus not significant. Most values of *c and V* plot on the ideal mixing lines and connecting the 450°C alunite and natroalunite samples, which have the equations

$$X_{Na} = (17.331 - c_{meas})/0.635 \quad (12)$$

$$X_{Na} = (731.5 - V_{meas})/27.3 \quad (13)$$

If the uncertainty in the end-member values is also considered, all but four of the samples are within 2σ of ideal mixing. These samples do not define a systematic departure from ideal mixing and are believed to reflect errors in X_{Na} caused by compositional heterogeneity.

Mixing relations along the alunite-natroalunite binary were investigated in mineral-water Na-K exchange experiments by Stoffregen and Cygan (1990). The exchange reaction is

$$KAl_3(SO_4)_2(OH)_{6(s)} + Na^+_{(aq)} \Leftrightarrow NaAl_3(SO_4)_2(OH)_{6(s)} + K^+_{(aq)} \quad (14)$$

The starting fluid in these experiments contained 0.5 *m* $(Na,K)_2SO_4$, which provided the alkalis necessary to drive the exchange reaction and also helped to stabilize alunite, but did not eliminate incongruent dissolution of alunite by Reaction (5). Defining the distribution coefficient K_D for this exchange as $(X_{Na}/X_K)(m_{Na}/m_K)$ where X indicates the mole fraction in the solid and *m* the molality in the aqueous solution, gives the expression:

$$RT\ln K_D = \Delta G°_{r,P,T} + (dG_{xs,alun}/dX_{Na}) - (dG_{xs,soln}/dN_{Na}) \quad (15)$$

where $\Delta G°_{r,P,T}$ is the standard-state Gibbs free-energy change for the alkali-exchange reaction at a given pressure and temperature, the G_{xs} terms are the excess Gibbs free

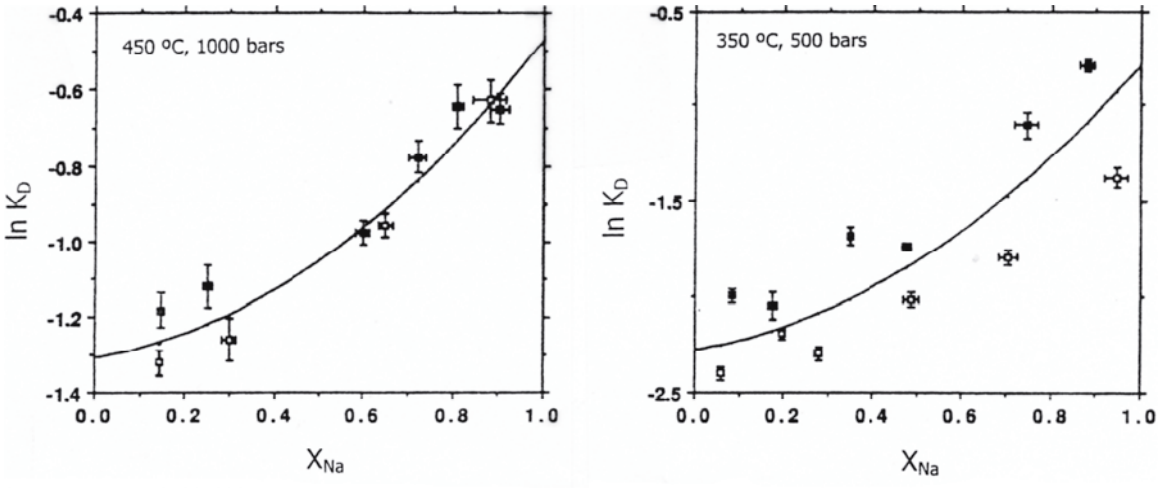

Figure 10 (upper left). Results of alunite-fluid Na-K exchange reactions at 450°C and 1000 bars. Open symbols = runs in which X_{Na} increased; filled symbols = runs in which X_{Na} decreased; curve represents subregular Margules model from the parameters listed in Table 4. From Stoffregen and Cygan (1990).

Figure 11 (above). Results of alunite-fluid Na-K exchange reactions at 350°C and 500 bars. Symbols and curve as in Figure 10. From Stoffregen and Cygan (1990).

Figure 12 (left). Results of alunite–fluid Na-K exchange reactions at 250°C and 500 bars. Symbols and curve as in Figure 10. From Stoffregen and Cygan (1990).

energy of mixing in the solid and in the aqueous solution, X_{Na} is the mole fraction of Na in the solid, and N_{Na} is the molar Na/(Na+K) ratio in the aqueous solution. Stoffregen and Cygan (1990) assumed that the excess free energy of mixing in the fluid, which is equal to the difference in the activity coefficients for Na and K, was negligible and could be ignored.

Experimentally derived values of $1nK_D$ are plotted against X_{Na} at 450, 350, and 250°C in Figures 10, 11, and 12, respectively. Stoffregen and Cygan (1990) fit these data using a subregular Margules model which assumes that the excess free energy of the solid can be expressed as $G_{xs} = X_K X_{Na}(W_{Na}X_K + W_K X_{Na})$. This model is necessary to describe the nonlinear variation in $1nK_D$ with X_{Na} that is evident in the figures.

Table 4 lists the parameters of fit for the excess mixing terms. The uncertainty in these terms increases with decreasing temperature, reflecting the poorer quality of the reversals at lower temperature. The data nevertheless indicate that the mixing terms increase with decreasing temperature. This behavior is typical of many solid solutions

Table 4. Alunite-natroalunite mixing parameters (from Stoffregen and Cygan 1990).

	LnK	$W_{G,Na}$	$W_{G,K}$
450 °C, 1000 bars	–0.99(0.05)	1,837(427)	3159(435)
350 °C, 500 bars	–1.73(0.26)	2,867(1050)	4785(1229)
250 °C, 500 bars	–2.56(0.42)	4,668(2091)	6443(4836)

W terms in J/mol

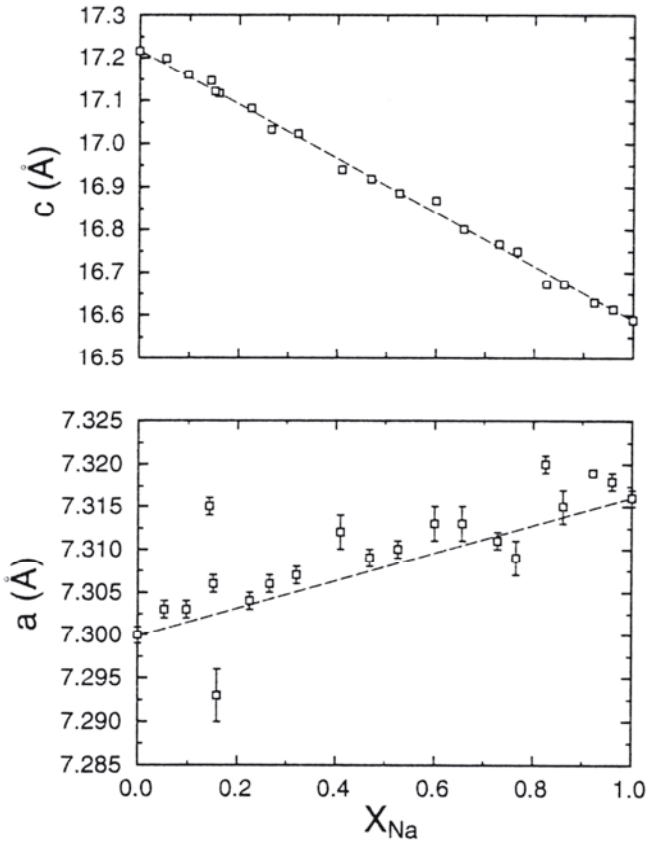

Figure 13. Unit-cell parameters of synthetic jarosite (200°C) as a function of Na mole fraction (Stoffregen, unpublished data).

(e.g. Powell 1974) and favors the formation of a solvus between alunite and natroalunite as temperature decreases. This solvus cannot occur at or above 350°C, at which the experimental results demonstrate complete miscibility, but the results do not preclude a miscibility gap at 250°C. As is discussed below, data on the chemistry of natural alunite also suggest a miscibility gap.

Jarosite-natrojarosite. Unit-cell dimensions for 19 samples of jarosite of intermediate composition prepared in jarosite-water Na-K exchange reactions at 200 and 250°C are plotted as a function of composition in Figure 13. Also included in Figure 13 are data for end-member jarosite and natrojarosite. Unlike alunite, the *a* unit-cell dimension of jarosite appears to increase from the K to Na end-members, with the latter larger by about 0.015 Å. Values of *c* and *V* define the following two least-squares relationships:

$$X_{Na} = (17.222 - c_{meas})/0.635 \quad (16)$$

$$X_{Na} = (795.20 - V_{meas})/25.9 \quad (17)$$

The slope on Equation (16) is identical to that observed for alunite (Eqn. 12). Most of the samples plot within two standard deviations of the ideal mixing line. Thus, the data are adequately described by an ideal mixing model.

Mixing relations along the jarosite-natrojarosite binary were investigated in mineral–water Na-K exchange experiments at 150 to 250°C (Stoffregen 1993). The exchange reaction is

$$KFe_3(SO_4)_2(OH)_{6(s)} + Na^+_{(aq)} \Leftrightarrow NaFe_3(SO_4)_2(OH)_{6(s)} + K^+_{(aq)} \quad (18)$$

As with the exchange experiments for alunite as discussed above, the initial fluid in the experiments involving jarosite contained 0.5*m* $(Na,K)_2SO_4$. However, to remain within the field of stability of jarosite and natrojarosite, it was also necessary to include 1.0 *m* H_2SO_4 in the starting solution.

In relation to Reaction (18), $1nK_D$ is related to the Gibbs free energy of mixing in the solid phase by an expression analogous to Equation (15) above, except with an excess-free-energy term for jarosite instead of alunite. As discussed by Stoffregen (1993), the excess-free-energy term for the fluid may be assumed constant at a given temperature and H_2SO_4 and $(Na,K)_2SO_4$ concentration. This allows Equation (15) to be rewritten as

$$-RTlnK_D^* = + \Delta G^\circ_{P,T} + (dG_{xs,jar}/dX_{Na}) \quad (19)$$

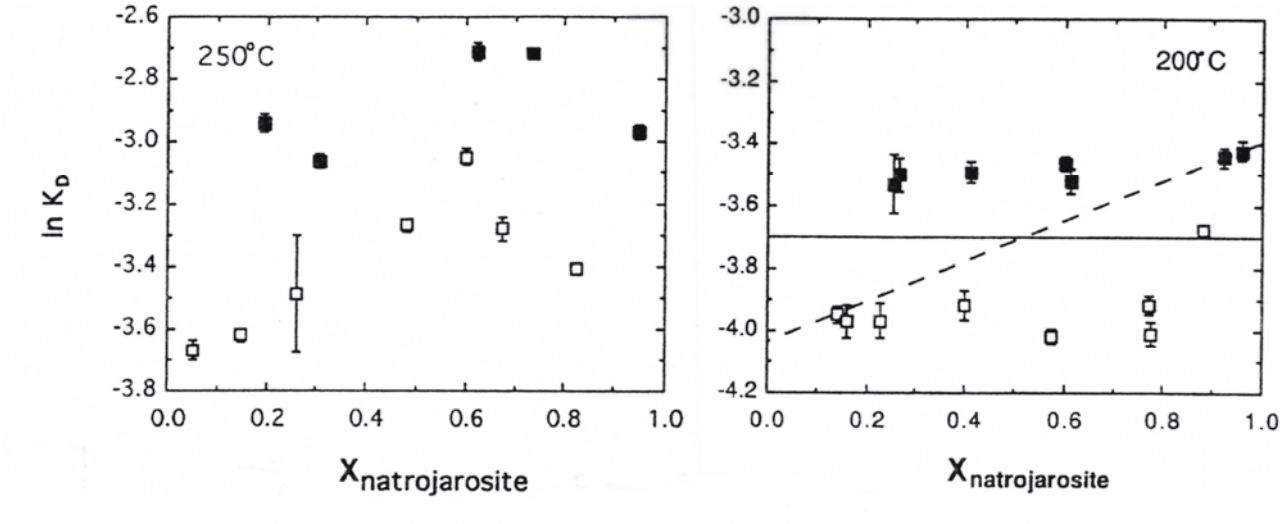

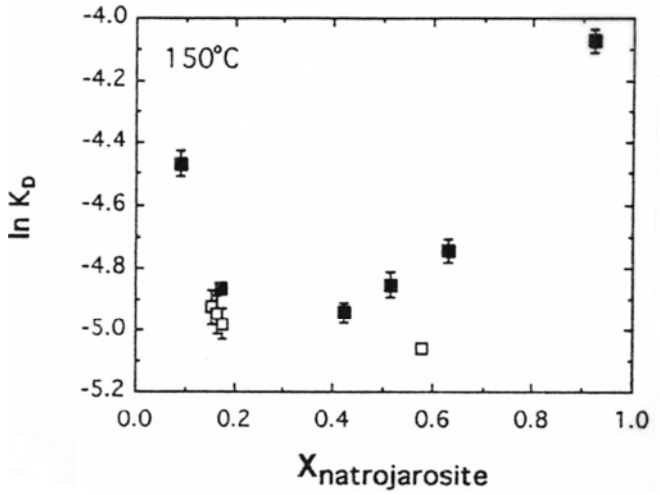

Figure 14 (upper left). Results of jarosite–fluid Na-K exchange reactions at 250°C, 100 bars. Open symbols = runs in which $X_{natrojarosite}$ increased; solid squares = runs in which $X_{natrojarosite}$ decreased. Used by permission of Elsevier Science Ltd., from Stoffregen (1993), *Geochim Cosmochim* Acta Vol. 57, Fig. 4(a), p. 2424.

Figure 15 (upper right). Results of jarosite–fluid Na-K exchange reactions at 200°C, 100 bars. Symbols as in Figure 14; dashed line was used to compute the largest value for the regular mixing term *W* permitted by the experimental data (see Stoffregen 1993); solid line shows position of $1nK_D$ for an ideal mixing model. Used by permission of Elsevier Science Ltd., from Stoffregen (1993), *Geochim Cosmochim Acta* Vol. 57, Fig. 4(b), p. 2424.

Figure 16 (above). Results of jarosite–fluid Na-K exchange reactions at 150°C, vapor saturation pressure. Used by permission of Elsevier Science Ltd., from Stoffregen (1993), *Geochim Cosmochim Acta* Vol. 57, Fig. 4(c), p. 2424.

where $1nK_D$* is the distribution coefficient corrected by a constant related to mixing in the fluid. For mH_2SO_4 = 1.0 and $m(Na,K)_2SO_4$ = 0.5, this constant is equal to 0.25 at 25°C and to 0.35 at 150°C and 200°C as calculated with PHRQPITZ (Plummer et al. 1988).

Experimental results at 250, 200, and 150°C are presented in Figures 14, 15 and 16, respectively. The best constraints on the value of $1nK_D$ for Reaction (18) are provided by the experiments at 200°C (Fig. 15). After correction for excess mixing in the fluid phase, these experiments indicate that $1nK_D$* is between -3.8 and -4.4 over the compositional range of X_{Na} = 0.14 to 0.96. This data set is consistent with, but does not require, ideal mixing along the jarosite-natrojarosite binary, for which $1nK_D$* is a constant.

The maximum departure from ideal mixing consistent with these data can be evaluated by assuming that jarosite and natrojarosite obey a regular solution model. The excess mixing term ($dG_{xs,jar}/dX_{Na}$) in this model is equal to $W(1 - 2X_{Na})$, which implies that $1nK_D$* is a linear function of X_{Na}. The maximum value of *W* consistent with the 200°C data is 1275 J/mole, which was obtained by connecting the values for $1nK_D$ at X_{Na} from 0.14 to 0.96 as illustrated in Figure 15. For comparison, *W* must exceed 7800 J/mole

for a solvus to occur at 200°C. Thus, although the experimental reversals at 200°C do not preclude some departure from ideality on the jarosite-natrojarosite binary, they demonstrate that the degree of non-ideality is small compared to that required for a solvus.

The experimental data presented above on alkali exchange in jarosite and natrojarosite demonstrate that the minerals form a nearly ideal solid solution at 200°C. This is substantially different from the alunite-natroalunite binary, which could have an asymmetric solvus at a temperature as high as 250°C, as was discussed above. The nearly ideal behavior of jarosite and natrojarosite at 200°C strongly suggests that there is complete miscibility on the jarosite-natrojarosite binary down to 25°C. Support for this suggestion is that data on natural and synthetic jarosite from a number of sources include compositions throughout the jarosite - natrojarosite - hydronium jarosite ternary (Brophy and Sheridan 1965, Alpers et al. 1989). However, these data do not provide conclusive proof of complete miscibility in this system for the following reasons: (1) amongst the samples analyzed by bulk chemical methods there may be samples that are, in reality, mixtures of two chemically distinct jarosites, and (2) the compositions may reflect non-equilibrium processes.

Alunite-jarosite. The only published studies of mixing between alunite and jarosite are those of Brophy et al. (1962) and Härtig et al. (1984). Brophy et al. (1962) synthesized a range of intermediate compositions in the series $K(Al,Fe)_3(SO_4)_{2(}OH)_6$ at 78, 105, and 150°C using 0.2 N sulfuric acid solutions. Recognizing the tendency for a deficiency of trivalent ions and an excess of water in alunite and jarosite synthesized at low temperature, Brophy et al. (1962) removed the excess water by heating to 300°C. Härtig et al. (1984) synthesized nine intermediate compositions in the series $K(Al,Fe)_3(SO_4)_2(OH)_6$ using mixed solutions of Fe–Al–K sulfate at 100°C, with an initial pH of 2.0. The solids produced in the experiments of Härtig et al. (1984) were non-stoichiometric with regard to (Al+Fe):S molar ratios, which ranged from 2.20:2 to 2.57:2. In both studies, for a given Al/(Al+Fe) ratio in the initial solution, the alunite-jarosite solid solution had a higher Fe content, which is expected because Fe^{3+} hydrolyzes at a lower pH than does Al^{3+}. The solids produced in both studies followed Vegard's rule with regard to the *a* unit-cell dimension, which varies from about 6.98 Å in alunite to about 7.30 Å in jarosite. Little to no variation in the *c* unit-cell dimension was observed.

Few data are available on the Al content of natural jarosite the Fe content of natural alunite. Brophy et al. (1962, and references therein) reported the compositions of four samples of alunite, three samples of jarosite, and one sample with equimolor amounts of Al and Fe, from Kopec, Czech Republic (Jirkovsky 1927). An alunite of composition $K(Al_{0.87}Fe_{0.13})_3(SO_4)_2(OH)_6$ from the Copper Cap uranium prospect, Marysvale, Utah, was reported by Brophy et al. (1962). Unit-cell dimensions reported by Brophy et al. (1962) for the samples from Kopec and Copper Cap are consistent with those of synthetic solids of similar composition, indicating that unit-cell dimensions (especially *a*) can be used to make reliable estimates of Fe–Al substitution in the alunite-jarosite series. Alpers et al. (1992) used the cell dimensions of alunite and jarosite from Lake Tyrrell, Australia, together with chemical data, to estimate solid-solution compositions of approximately $[K_{0.87}Na_{0.04}(H_3O)_{0.09}](Al_{0.92}Fe_{0.08})_3(SO_4)_2(OH)_6$ for alunite and $[K_{0.89}Na_{0.07}(H_3O)_{0.04}](Fe_{0.80}Al_{0.20})_3(SO_4)_2(OH)_6$ for jarosite.

Geochemical modeling of alunite and jarosite formation (e.g. Bladh 1982) has generally considered alunite and jarosite to be distinct phases rather than members of a solid-solution series. Whether a miscibility gap exists between alunite and jarosite remains unknown, though it appears to be unlikely. It is more likely that the chemical separation of Fe and Al and the rarity of intermediate compositions in the alunite-jarosite

series is caused primarily by the difference in hydrolysis constants between $Fe^{3+}_{(aq)}$ and $Al^{3+}_{(aq)}$ (Brophy et al. 1962, Nordstrom and Alpers 1999, Bigham and Nordstrom, this volume).

GEOCHEMISTRY AND OCCURRENCES

Alunite and natroalunite

Substitutions. The most significant substitution in natural alunite is that of Na^+ for K^+ on the alkali site. Hydronium (H_3O^+) substitution is difficult to prove, but has been inferred for most samples of synthetic alunite and most low-temperature natural alunite samples because of a deficiency in alkalis and an excess of water compared with the stoichiometric composition (e.g. Ripmeester et al. 1986). The non-stoichiometric water is generally attributed to the presence of hydronium (H_3O^+) but may also reflect other forms of "excess water" as discussed by Ripmeester et al. (1986). Another substitution that occurs in alunite is the coupled substitution of phosphate (or arsenate) and a divalent cation for sulfate and a monovalent cation, as described by the exchange reaction

$$SO_4^{2-} + D^+ \Leftrightarrow PO_4^{3-} + D^{2+} \quad (20)$$

The minerals woodhouseite and svanbergite consist of the alunite structure in which PO_4^{3-} substitutes for 25-75% of the total formula SO_4^{2-} and the divalent cations Ca^{2+} and Sr^{2+}, respectively, predominate on the *D* site. There are a few published studies that discuss the extent of the coupled substitution represented by Reaction (20) in alunite. Significant solid solution between alunite and woodhouseite-svanbergite has been documented by Wise (1975), who observed a "strontian natroalunite" with about 12 formula % PO_4^{3-} in substitution for SO_4^{2-} and a corresponding amount of Sr^{2+} substitution for Na^+. Stoffregen and Alpers (1987) reported that alunite from the Summitville gold deposit in Colorado shows low phosphate, Ca, and Sr contents. Alunite from La Escondida, a porphyry copper deposit in northern Chile, is somewhat richer in phosphate and Sr than are the Summitville samples.

Stoffregen and Alpers (1987) also analyzed alunite from three other localities: La Tolfa, Italy; Marysvale, Utah; and Goldfield, Nevada. La Tolfa is a hot-springs deposit, in which alunite is believed to have formed at or near the surface (Lombardi and Barbieri 1983). The alunite analyzed from Marysvale is interpreted to be of magmatic-steam origin (Cunningham et al. 1984, Rye et al. 1992). The alunites from both La Tolfa and Marysvale are not thought to be directly related to precious-metal mineralization (Lombardi and Barbieri 1983, Cunningham et al. 1984). In contrast, Goldfield, Nevada is a magmatic-hydrothermal, gold–sulfosalt deposit similar to that at Summitville, Colorado (Ashley 1974). Alunite analyzed by Stoffregen and Alpers (1987) from La Tolfa and Marysvale has significant and fairly consistent SrO and P_2O_5 contents (samples 3 and 4 in Table 5). Alunite from Goldfield (sample 5 in Table 5) contains up to 0.20 wt % BaO but has no detectable Sr and only 0.05 wt % P_2O_5.

Allibone et al. (1995) determined that advanced argillic alteration assemblages at the Temora mine in New South Wales, Australia, contain alunite, natroalunite, woodhouseite, and svanbergite. Analyses plotted by Allibone et al. (1995) show an almost continuous increase in PO_4 that is commensurate with substitution of divalent cations (Ca, Sr, Ba) for monovalent cations (Na, K). Overall, however, the results from the various deposits suggest a limited degree of this coupled substitution in samples of magmatic-related, hypogene alunite formed at temperatures below about 300°C, although solid solution at higher temperatures is more extensive. Grains of woodhouseite, svanbergite, and related phases are found, in some cases, replacing apatite in zones of advanced argillic alteration (Stoffregen and Alpers 1987); the availability of phosphate

Table 5. Chemical composition of hydrothermal alunite (from Stoffregen and Alpers 1987).

	1	2	3	4	5
Weight %					
K_2O	7.49	9.18	10.79	10.84	9.66
Na_2O	2.41	1.44	n.d.	0.19	1.04
CaO	n.d.	n.d.	n.d.	n.d.	0.05
SrO	0.05	0.34	0.38	0.31	n.d.
BaO	n.a.	n.d.	n.d.	n.d.	0.20
Al_2O_3	37.34	36.50	36.70	36.92	37.13
SO_3	38.44	38.67	37.07	36.94	37.96
P_2O_5	0.23	0.30	0.63	0.86	0.05
H_2O[a]	13.20	13.05	13.05	13.05	13.10
Total	99.16	99.78	98.62	99.11	99.19
Moles					
K	0.656	0.505	0.961	0.952	0.853
Na	0.321	0.192	n.d.	0.024	0.139
Ca	n.d.	n.d.	n.d.	n.d.	0.003
Sr	0.002	0.014	0.016	0.012	n.d.
Ba	n.d.	n.d.	n.d.	n.d.	0.005
Al	3.017	2.980	3.021	2.998	3.029
S	1.978	1.994	1.944	1.91	1.975
P	0.013	0.018	0.036	0.049	0.002
OH[b]	6.048	5.981	6.080	6.003	6.034

[a] wt % H_2O calculated based on elemental composition and stoichiometry of end-member minerals in alunite supergroup (see Stoffregen and Alpers 1987)

[b] moles OH calculated based on wt % H_2O

n.d. = not detected; n.a = not analyzed for.

Description of alunite samples: 1. Summitville, Colorado (255-629), 2. La Escondida, Chile (1067-C-298), 3. La Tolfa, Italy, 4. Marysvale, Utah, 5. Goldfield, Nevada

(and arsenate) may be the main limiting factor in determining the extent of solid solution by Reaction (20). In the high-alumina rocks east of Lake Baykal, Russia, Ripp and Kanakin (1998) and Ripp et al. (1998) have shown extensive solid solution of PO_4 in predominantly Sr-substituted natroalunite (Fig. 17). Muscovite in the prograde metamorphic assemblage was formed at 520-600°C and >5 kbar, but the associated minerals of the alunite supergroup were formed in the retrograde stage (Ripp et al. 1998).

Occurrences. Stoffregen and Alpers (1992) subdivided natural alunite into four groups on the basis of their grain size, mode of occurrence, and morphology: disseminated, coarse vein, porcelaneous vein, and fine-grained. Disseminated alunite occurs in bladed crystals 1 to 10 mm in length, which replace feldspar grains and which are accompanied by quartz and fine-grained disseminated pyrite. Coarse vein alunite occurs in >1 mm crystals in nearly monomineralic veins or pods which may be up to several meters in width. Porcelaneous vein alunite occurs as 5 to 100 μm grains with irregular surfaces within veinlets a few millimeters to a few centimeters wide and may be accompanied by minor quartz and kaolinite. Fine-grained alunite occurs as 0.5 to 5 μm pseudocubic grains within veinlets, small concretions, or bedded sediments. Fine-grained

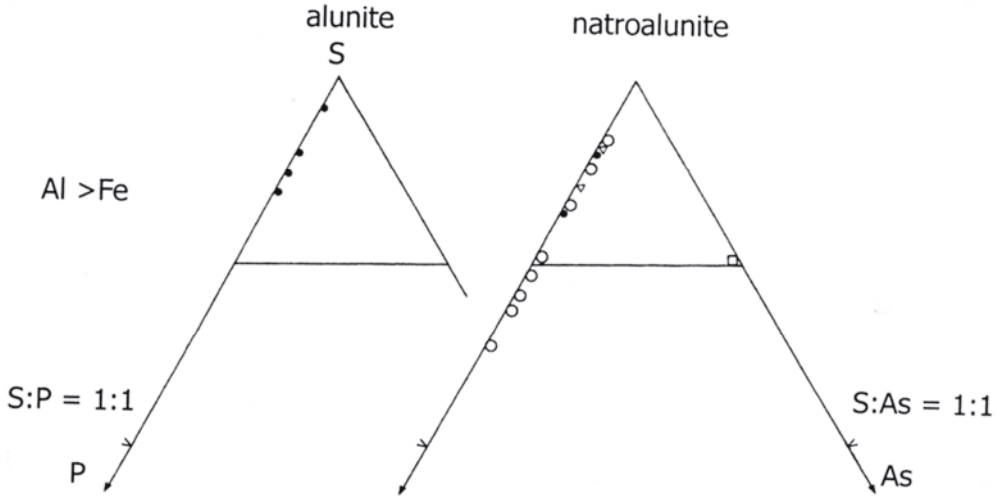

Figure 17. Compositions of PO_4-substituted alunite and natroalunite. The compositional fields for alunite and natroalunite are according to the current nomenclature system (Scott 1987); S:P = 1:1 and S:As = 1:1 indicate formula SO_4:PO_4 = 1:1 and SO_4:AsO_4 = 1:1, respectively. Data points for alunite are from Allibone et al. (1995), and sources for natroalunite are: open circles, Ripp et al. (1998) and Ripp and Kanakin (1998); triangles, Wise (1975); solid circles, Allibone et al. (1995). The open square on the far right represents the AsO_4:SO4 composition of type schlossmacherite (Schmetzer et al. 1980).

alunite is generally formed at low temperature, but temperature may not be the only factor affecting grain size.

Sedimentary and low-temperature alunite. Fine-grained alunite seems to be limited to near-surface environments. This type of alunite has been reported from weathered profiles (e.g. Meyer and Peña dos Reis 1985), intertidal marine environments (e.g. Khalaf 1990), lacustrine environments (e.g. Alpers et al. 1992), and caves (e.g. Polyak et al. 1998). Porcelaneous vein alunite may form at low temperature, as illustrated by the alunite from Round Mountain, Nevada, which has been interpreted as supergene by Fifarek and Gerike (1991) and Rye et al. (1992).

Most fine-grained alunite described to date, including the three specimens investigated by Stoffregen and Alpers (1992), contain between 14 and 16 wt % H_2O. This corresponds to between 5 and 35 mol % H_3O^+ on the alkali site if all non-hydroxyl water is assumed to be present as hydronium. More hydronium-rich, fine-grained alunites, including possibly schlossmacherite (hydronium-dominant alunite) have also been reported. The common occurrence of non-hydroxyl water in fine-grained alunite suggests that at near-surface temperatures, fluid [H_3O^+/(Na+K)] ratios are generally large enough to stabilize some hydronium component in alunite.

Low-temperature alunite is characterized by relatively large unit-cell values for *a*, which as discussed above, are interpreted to result from hydronium substitution. This substitution can be detected in XRD data, as illustrated in Figure 18. Values of *a* show no systematic variation with X_{Na}, but most of the fine-grained and porcelaneous vein alunite has values for *a* that are larger than those of the other natural specimens and the synthetic samples prepared at 450°C. These anomalously high values of *a* may reflect the presence of non-hydroxyl water, but they may also be an indication of Fe^{3+}-for-Al substitution, which also causes an increase in *a* (Brophy et al. 1962).

Figure 18 also shows, on the basis of the *c* unit-cell dimension, a range of Na contents from pure alunite to pure natroalunite at low temperature. However, intermediate compositions are not common.

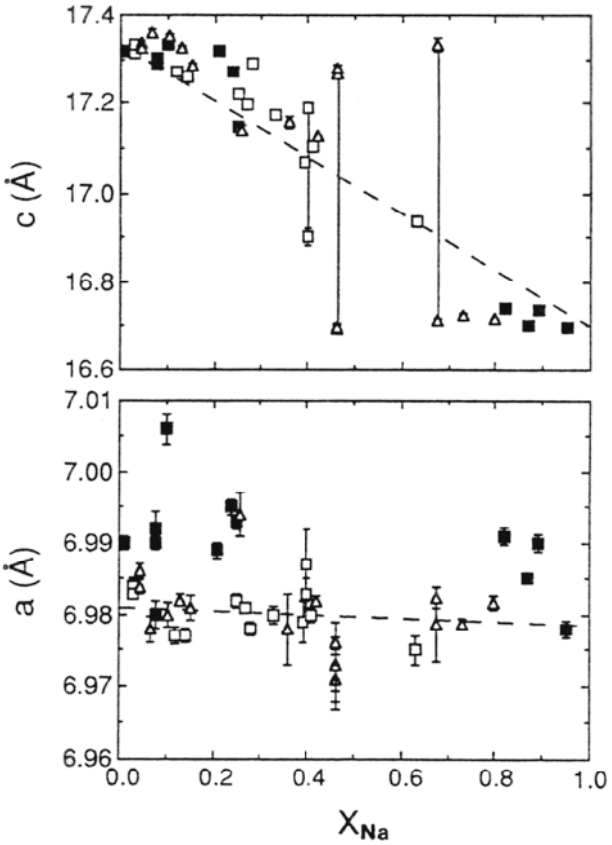

Figure 18. Unit-cell parameters of natural alunite as a function of Na mole fraction. Open squares are disseminated and coarse vein alunite, solid squares are porcelaneous vein and fine-grained alunite, and open triangles are unclassified. Vertical lines connect alunite pairs from the same specimen. Dashed lines connect values for synthetic end-members, as shown in Figure 9. Errors (1σ) are less than the symbol size except where shown. From Stoffregen and Alpers (1992).

Hydrothermal. Porcelaneous vein alunite can occur in hot-spring environments, as demonstrated by a specimen from the modern-day Waiotapu geothermal field included in the data set shown in Figure 18. Disseminated alunite forms at 200-300°C as determined by isotope geothermometry and corroborative geological evidence (Rye et al. 1992). Although formation temperatures for coarse vein alunite are not well-constrained, they are likely to be similar to those of disseminated alunite on the basis of the common spatial association of the two alunite types.

Magmatic-hydrothermal alunite characteristically occurs intimately intergrown with fine-grained disseminated pyrite in what is commonly interpreted as an equilibrium assemblage. This association, with quartz and commonly with kaolinite, is the classic "advanced argillic" assemblage of Meyer and Hemley (1967), described from many hydrothennal ore deposits. A higher temperature variant includes pyrophyllite.

The large overlap between the stability fields of alunite and pyrite is consistent with the common association of alunite and pyrite in volcanic-hydrothermal environments at temperatures in excess of 200°C (e.g. Rye et al. 1992). Log f_{O_2} in these environments is generally buffered on or near $HSO_4^- - H_2S$ equivalence by the influx of magmatic SO_2 and H_2S (e.g. Rye et al. 1992).

Some alunite from modern geothermal areas also contains hydronium (e.g. Aoki 1983), which suggests that a hydronium component may be stable to at least 100°C. Such stability is consistent with the presence of non-hydroxyl water in alunite and natroalunite synthesized at 150°C. However, as the non-hydroxyl water in these and the fine-grained natural alunite may also be a non-equilibrium effect, such water does not prove that a hydronium component is stable in alunite at any temperature. The absence of non-hydroxyl water in disseminated alunite, as indicated by H_2O determinations and by the

lack of the anomalous values of unit-cell *a*, strongly suggests that a hydronium alunite component is not stable above 200°C. This temperature limit is consistent with the observed decrease in water content of synthetic 150°C alunite and natroalunite when heated to 250 and 450°C.

Figure 18 includes data for four natural samples that are mixtures of two alunites with different X_{Na}. The bulk X_{Na} for these specimens is between 0.40 and 0.70, but the unit-cell data indicate that three of the four are mixtures of relatively pure alunite and natroalunite. In the fourth sample, from Summitville, Colorado, alunite compositions of X_{Na} = 0.68 and 0.23 were determined from the XRD data. It is interesting to note that coarse vein alunite from Komatsuga, Japan, and disseminated alunite from Goldfield, Nevada, are the only specimens studied, besides the more sodic Summitville alunite, that are within the range of X_{Na} = 0040 and 0.70 on the basis of Equation (12). The absence of fine-grained and porcelaneous vein alunite in this range may reflect a miscibility gap between alunite and natroalunite, a possibility also suggested by the experimental data on alunite-natroalunite mixing discussed above.

Metamorphic alunite. Alunite and natroalunite have been reported in low- to intermediate-grade, Al-rich metamorphic rocks that have no obvious hydrothermal affinities. The best documented of these occurrences are from the White Mountains of California (Wise 1975), from South Africa (Schoch et al. 1989), and from Russia (Ripp et al. 1998). At the South African locality, natroalunite occurs "as alteration veins and incrustations in massive sillimanite bodies which form part of a biotite–sillimanite schist." Quartz is not reported. The natroalunite contains only 1-6 mol % K but shows up to 18 mol % Ca and small amounts of phosphate.

No formation temperatures are reported for the alunite-supergroup minerals within these paragenetic associations. However, the association with rocks that may be generalized as of intermediate metamorphic grade suggests that alunite and natroalunite may persist in rare instances to temperatures in the range of 400 to 500°C if bulk-rock compositions are favorable. It is likely that fluid flow through such rocks was inhibited, as a significant flux of water would remove the alunite through reactions of the generalized form alunite → aluminosilicate + H_2SO_4. The alunite in these environments generally contains partial phosphate substitution for sulfate (e.g. Fig. 17), which suggests increased miscibility among the members of the group at the higher temperatures of origin inferred for this environment.

Jarosite and natrojarosite

Substitutions. Like alunite, the most common substitutions in jarosite are Na and H_3O on the alkali site. Hydronium substitution seems to be more common in jarosite than in alunite formed at similar temperature (Dutrizac and Kaiman 1976, Dutrizac and Jan1bor, this volume). This may be correlated with the fact that solutions that form jarosite are generally of lower pH (greater hydronium activity) compared with those that form alunite. Although plumbojarosite and argentojarosite (Table 1) occur only rarely in great abundance, these minerals and Pb- and Ag-bearing jarosite solid solutions may play a role in limiting the concentration of Pb and Ag in acidic waters such as mine drainage (e.g. Hochella et al. 1999).

Occurrences. Jarosite is common in weathering environments, where it forms as a supergene product of Fe-sulfide oxidation, but occurrences of jarosite in hydrothermal environments are uncommon (see Dutrizac and Jambor, this volume). Jarosite is generally absent as a hypogene mineral even in the sulfur-rich volcanic-hydrothermal systems that produce extensive zones of alunitic alteration. Supergene jarosite may replace alunite of either hypogene or supergene origin in situations where fluids become

either more acidic or more oxidizing, or both. A mechanism for this type of evolution is long-term descent of the water table in response to erosion or climatic fluctuation. Hypogene or supergene alunite tends to form at or below the water table, and then jarosite forms in association with acidic, oxidizing conditions most commonly associated with the weathering of sulfide minerals.

The Paradise Peak Au–Ag–Hg deposit in Nevada contains perhaps the best documented example of hydrothermal jarosite. John et al. (1991) suggested that relatively coarse crystals (~ 2 mm) of jarosite occurring as a breccia matrix at Paradise Peak were formed at shallow depth (<200 m) over a temperature range of 150-200°C. This range is consistent with a formation temperature of 150°C that was obtained from the fractionation of ^{18}O between the sulfate and hydroxyl sites in this jarosite (Stoffregen et al. 1994). Other possible examples of hydrothermal jarosite occur in the Marysvale Volcanic Field, and are believed to have formed in a near-surface geothermal environment similar to that inferred for Paradise Peak (Cunningham et al. 1984). Polycrystalline masses of jarosite, up to 10 cm in size, at the Apex germanium-gallium mine in Utah have been described by Mahin (1990). On the basis of this coarse grain size, and on data from fluid inclusions, Mahin (1990) argued that jarosite in the Apex mine may have formed at a temperature of 200°C. Coarsely crystalline jarosite from Gilbert, Nevada, gave a formation temperature of 150°C (Rye and Alpers 1997) on the basis of ^{18}O fractionation between the sulfate and hydroxyl sites (Stoffregen et al. 1994). Such jarosite occurrences in the range of 150-200°C require fluids that were highly oxidizing and rich in sulfuric acid, and which were present roughly 20 to 100 m below the water table in these deposits. Another occurrence of coarsely crystalline jarosite, likely of hydrothermal origin, is known from the uranium deposit at Peña Blanca, Chihuahua, Mexico (P. Goodell, unpublished data).

The relatively rare occurrence of jarosite in hydrothermal environments is consistent with the experimental data described above, which demonstrate that jarosite requires more extreme acidity and more oxidizing conditions to form than does alunite. The jarosite-pyrite phase boundary lies more than two log units above the line in log f_{O_2} space representing equal activities of HSO_4^- and H_2S in the aqueous phase. As log f_{O_2} in volcanic environments is generally buffered on or near HSO_4^-–H_2S equivalence by the influx of magmatic SO_2 and H_2S (Rye et al. 1992), jarosite cannot be stabilized regardless of the pH attained in the system.

GEOCHRONOLOGY USING ALUNITE AND JAROSITE

The large concentration of K in alunite and jarosite makes these minerals potentially useful for age determinations by K-Ar and $^{40}Ar/^{39}Ar$ methods. Because both alunite and jarosite may form at either high- or low-temperature conditions, these minerals can provide information on the geochronology of both hydrothermal systems and weathering profiles. The multiple crystallographic sites available for measurement of stable isotopes in alunite and jarosite (S, H, O_{OH}, and O_{SO_4}) make weathering-related alunite and jarosite desirable candidates for paleoenvironmental studies because the direct radiometric dating of the minerals can be coupled with information about the stable isotopes of the meteoric waters from which the minerals formed (see Seal et al., this volume). This section provides an overview of the literature on K-Ar and $^{40}Ar/^{39}Ar$ methods as applied to alunite and jarosite. For additional details on geochronology using alunite and jarosite, see the recent, comprehensive reviews by Vasconcelos (1999a,b).

The first published K-Ar dates on alunite were by Shanin et al. (1968), Webb and McDonald (1968), and Chuchrov et al. (1969). Silberman and Ashley (1970) presented data on hydrothermal alunite from the epithermal gold deposit at Goldfield, Nevada, as

part of a stratigraphically controlled study that provided the first geological evidence of the suitability of alunite for K-Ar dating. Argon-release experiments by Itaya et al. (1996) have since confirmed that both coarse-grained, hypogene alunite and fine-grained, supergene alunite are suitable for K-Ar dating.

Among additional studies that have used K-Ar dating of alunite to date hydrothermal events and associated precious- and base-metal mineralization are those by Mehnert et al. (1973), Ashley and Silberman (1976), Steven et al. (1979), Whalen et al. (1982), Pécksay et al. (1986), Alpers and Brimhall (1988), John et al. (1989), Sillitoe et al. (1991), Perello (1994), and Arribas et al. (1995a,b). An important factor in the interpretation of K-Ar data for hypogene alunite is the need for careful paragenetic analysis to determine the relationship between alunite deposition and sulfide mineralization. Although alunite and pyrite may be co-deposited, the acid-sulfate conditions associated with formation of hypogene alunite (and more rarely, hypogene jarosite; see Dutrizac and Jambor, this volume) are generally not simultaneous with the deposition of ore sulfides or gold. The acid-sulfate (or advanced argillic) hydrothermal alteration with which hydrothermal alunite is associated can set the stage for later mineralization by establishing permeability in the host rocks, such as the vuggy silica alteration at Sunlmitville, Colorado (Stoffregen 1985).

The first K-Ar dating of supergene alunite from a porphyry copper deposit was reported by Gustafson and Hunt (1975) for EI Salvador, Chile. They reported ages of roughly 36 Ma for two samples, in contrast with an age of about 39 Ma for hypogene alunite from advanced argillic alteration; other hypogene minerals indicated that the main hydrothermal system was active from about 42-40 Ma. Gustafson and Hunt (1975) inferred that the main period of supergene oxidation and enrichment of Cu-sulfide ores took place within about 5 Ma of the hypogene mineralization. Also reported was that five samples of supergene jarosite gave ages of less than 21 Ma, with two younger than the 10-13 Ma gravels that cap the erosional surface; thus, it was interpreted that even coarsely crystalline jarosite does not retain Ar well enough to be useful for K-Ar dating. Another interpretation of these data is that jarosite at El Salvador may have been dissolved and recrystallized in response to periodic influxes of meteoric water.

Alpers and Brimhall (1988) used K-Ar dates on supergene alunite from the porphyry copper deposit at La Escondida, Chile, to determine that supergene-Cu enrichment took place about 15-18 million years ago. K-Ar dates for hypogene alteration minerals from La Escondida reported by Alpers (1986), Ojeda (1986), and Alpers and Brimhall (1988), including two dates on hypogene alunite, indicated that the hydrothermal system was active between about 31 and 39 Ma. More recent studies by Richards et al. (1999) at La Escondida and the adjacent deposits of Zaldívar and Chimborazo, using U-Pb on zircon and the more precise $^{40}Ar/^{39}Ar$ methods on biotite, have suggested that primary mineralization and alteration was most important around 38 Ma, and that non-mineralizing systems continued to be active until 31 Ma. Alpers and Brimhall (1988) used K-Ar dates from supergene alunite to infer that regional climate change, resulting in the present hyper-arid conditions in the Atacama Desert, the lowering of long-term erosion rates, and the preservation of the supergene-enriched Cu deposits, was caused by uplift of the central Andes as well as intensification of the Humboldt Current related to build-up of the Antarctic ice cap during the middle Miocene. On the basis of results from analyses of 25 samples of supergene alunite from porphyry copper deposits in northern Chile, Sillitoe and McKee (1996) reached a similar conclusion to that of Alpers and Britnhall (1988), namely, that supergene processes were most active between 34 and 14 Ma, and that intensifying aridity related to regional uplift was the most likely reason for cessation of enrichment and preservation of the supergene deposits. K-Ar dates of

supergene alunite from porphyry copper deposits in southwestern North America were provided by Cook (1994).

The K-Ar and $^{40}Ar/^{39}Ar$ methods have been used to analyze supergene alunite from several gold deposits, including breccia-hosted deposits in Queensland, Australia (Bird et al. 1990), epithermal deposits in Nevada (Ashley and Silberman 1976, Tingley and Berger 1985, Sander 1988, Arehart and O'Neil 1993, Sillitoe and Lorson 1994, Vasconcelos et al. 1994), and sediment-hosted (Carlin-type) deposits, also in Nevada (Bloomstein et ai. 1990, Ilchik 1990, Sillitoe and Bohnam 1990, Arehart et al. 1992, 1993; Heitt 1992, Williams 1992, Arehart and O'Neil 1993, Teal and Branham 1997). The range for 30 published K-Ar dates of supergene alunite from the Carlin-type deposits is 3.6±0.2 to 30.0±1.2 Ma (Hofstra et ai. 1999). Hypogene mineralization in the Carlin Trend and the Battle Mountain-Eureka Belt is thought to have taken place between about 35 to 45 Ma (Hofstra et al. 1999).

Several studies of alunite and jarosite have combined the use of geochronology and stable isotopes to provide information about paleoclimate. An important development that has allowed these studies to reconstruct the stable isotopic composition of paleo-meteoric waters was the determination of fractionation factors for O and H for the alunite–water and jarosite–water systems (see Seal et al., this volume, and references therein). Bird (1988) and Bird et al. (1989, 1990) analyzed surficial alunite from the Australian regolith and concluded that recrystallization under moist conditions might complicate the interpretation of weathering profiles. Arehart and O'Neil (1993) used the stable isotopes of supergene alunite, coupled with K-Ar dates, to reconstruct the history of paleo-meteoric waters in Nevada for the past 30 million years (see Seal et al., this volume). Vasconcelos et al. (1994) used the results of $^{40}Ar/^{39}Ar$ analysis of supergene jarosite and alunite from Goldfield, Nevada, to infer that a pervasive Middle to Late Miocene oxidation event occurred in the western USA, and they correlated this event with results from weathering profiles of similar age in western Africa, Brazil, and Chile. The epithermal Ag and base-metal deposits at Creede, Colorado, were studied using K-Ar age determinations and stable-isotope data on supergene alunite and jarosite (Rye et al. 2000). The age range of alunite was 4.8 to 3.1 Ma, whereas the range for jarosite was 2.6 to 0.9 Ma. The isotopic results and their interpretation with regard to paleoclimate and regional uplift are discussed by Seal et al. (this volume).

Vaconcelos (1999b) compiled available data for about 200 age determinations of supergene minerals (alunite, jarosite, and K-Mn oxides) by K-Ar and $^{40}Ar/^{39}Ar$ methods. Most published ages of alunite and jarosite fall within the past 20 Ma, with some as old as 92 Ma, whereas the published ages for K-Mn oxides are distributed fairly evenly over the last 60 Ma, with some ages to 100 Ma or older. It remains to be seen whether the clustering of radiometric ages of alunite and jarosite to the past 20 Ma reflects bias in the selection of study sites (predominantly Nevada and Chile), or whether there was a global increase in weathering rates during the Miocene. Regardless of the outcome, the future looks promising for alunite and jarosite to be increasingly useful on a global scale as indicators of weathering history, regional tectonic history, and paleoclimate.

REFERENCES

Allibone AH, Cordery OR, Morrison OW, Jaireth S, Lindhorst JW (1995) Synchronous advanced argillic alteration and deformation in shear-hosted magmatic hydrothermal Au-Ag deposit at the Temora (Gidginbung) mine, New South Wales, Australia. Econ Geol 90:1570-1603

Alpers CN (1986) Geochemical and geomorphological evolution of supergene copper sulfide ore formation and preservation at La Escondida, Antofagasta, Chile. PhD thesis, University of California, Berkeley, California

Alpers CN, Brimhall GH (1988) Middle Miocene climatic change in the Atacama Desert, northern Chile: Evidence from supergene mineralization at La Escondida. Geol Soc Am Bull 100:1640-1656

Alpers CN, Nordstrom DK, Ball JW (1989) Solubility of jarosite solid solutions precipitated from acid mine waters, Iron Mountain, California, USA. Sci Géol Bull 42:281-298

Alpers CN, Rye RO, Nordstrom, DK, White LD, King BS (1992) Chemical, crystallographic and stable isotopic properties of alunite and jarosite from acid-hypersaline Australian lakes. Chem Geol 96:203-226

Aoki M (1983) Modes of occurrence and mineralogical properties of alunite solid solution in Osorezan geothermal area. Sci Rept Hirosake Univ 30:132-141 (in Japanese)

Arehart GB, O'Neil JR (1993) D/H ratios of supergene alunite as an indicator of paleoclimate in continental settings: Climate change in continental isotope records. Geophys Monograph 78:277-284

Arehart GB, Kesler SE, O'Neil JR, Foland KA (1992) Evidence for the supergene origin of alunite in sediment-hosted micron gold deposits, Nevada. Econ Geol 87:263-270

Arehart GB, Foland KA, Naeser CW, Kesler SE (1993) $^{40}Ar/^{39}Ar$, KlAr, and fission track geochronology of sediment-hosted disseminated gold deposits at Post-Betze, Carlin trend, northeastern Nevada. Econ Geol 88:622-646

Arribas A Jr, Cunningham CG, Rytuba JJ, Rye RO, Kelly WC, Podwysocki MH, McKee EH, Tosdal RM (1995a) Geology, geochronology, fluid inclusions, and isotope geochemistry of the Rodalquilar gold alunite deposit, Spain. Econ Geol 90:795-822

Arribas A Jr, Hedenquist JW, Itaya T, Okada T, Concepción RA, Garcia JS (1995b) Contemporaneous formation of adjacent porphyry and epithermal Cu-Au deposits over 300 ka in northern Luzon, Philippines. Geology 23:337-340

Ashley RP (1974) Goldfield mining district. *In* Guidebook to the Geology of Four Tertiary Volcanic Centers in Central Nevada. Nevada Bur Mines Geol Rept 19:49-66

Ashley RP, Silberman ML (1976) Direct dating of mineralization at Goldfield, Nevada, by potassium-argon and fission track methods. Econ Geol 71:904-924

Babcan J (1971) Die Synthese von Jarosit $KFe_3(SO_4)_2(OH)_6$. Geol Zbornik Geol Carpath 22:299-304

Baron D, Palmer CD (1996) Solubility of jarosite at 4-35 °C. Geochim Cosmochim Acta 60:185-195

Bird MI (1988) An isotopic study of the Australian regolith. PhD thesis, Australian National University, Canberra, Australia

Bird MI, Andrew AS, Chivas AR, Lock DE (1989) An isotopic study of surficial alunite in Austalia: 1. Hydrogen and sulfur isotopes. Geochim Cosmochim Acta 53:3223-3237

Bird MI, Chivas AR, McDougall I (1990) An isotopic study of surficial alunite in Australia: 2. Potassium-argon geochronology. Chem Geol 80:133-145

Bladh KW (1982) The formation of goethite, jarosite, and alunite during the weathering of sulfide-bearing felsic rocks. Econ Geol 77:176-184

Bloomstein EI, Massingill GL, Parratt RL, Peltonen DR (1990) Discovery, geology, and mineralization of the Rabbit Creek gold deposit, Humboldt County, Nevada. *In* Raines GL, Lisle RE, Schafer RW, Wilkinson WH (eds) Geology and Ore Deposits of the Great Basin. Symp Proc Geol Soc Nevada (Reno) 2:821-843

Brophy GP, Scott ES, Snellgrove RA (1962) Sulfate studies: II. Solid solution between alunite and jarosite. Am Mineral 47:112-126

Brophy GP, Sheridan MF (1965) Sulfate studies: IV. The jarosite-natrojarosite-hydronium jarosite solid solution series. Am Mineral 50:1595-1607

Chukhrov FV, Yermilova LP, Shanin LL (1969) Age of alunite from certain deposits. Trans Acad Sci USSR Dokl Earth Sci Sect 185:49-51

Cook SS III (1994) The geological history of supergene enrichment in the porphyry copper deposits of southwestern North America. PhD thesis, University of Arizona, Tucson, Arizona

Cunningham CG, Rye RO, Steven TA, Mehnert HH (1984) Origins and exploration significance of replacement and vein-type alunite deposits in the Marysvale volcanic field, west central Utah. Econ Geol 79:50-71

Dutrizac JE, Kaiman S (1976) Synthesis and properties of jarosite-type compounds. Can Mineral 14:151-158

Fifarek RH, Gerike GN (1991) Oxidation of hydrothermal sulfides at Round Mountain, Nevada: Origin and relation to gold mineralization. *In* Raines GL, Lisle RE, Schafer RW, Wilkinson WH (eds) Geology and Ore Deposits of the Great Basin. Symp Proc, Geol Soc Nevada (Reno) 2:1111-1121

Gustafson LB, Hunt JP (1975) The porphyry copper deposit at EI Salvador, Chile. Econ Geol 70:857-912

Härtig C, Brand P, Bohmhamrnel K (1984) Fe-Al Isomorphie und Strukturwasser in Kristallen von Jarosit-Alunit-Typ. Z anorg allg Chem 508:159-164

Heitt DG (1992) Characterization and genesis of alunite from the Gold Quarry mine, Eureka County, Nevada, and implications for Carlin-type mineralization. Soc Econ Geol Guidebook Ser 28:193-202

Helgeson HC, Delany JM, Nesbitt HW, Bird DK (1978) Summary and critique of the thermodynamic properties of rock-forming minerals. Am J Sci 278-A:1-229

Hemley JJ, Hostetler PB, Gude AJ, Mountjoy WT (1969) Some stability relations of alunite. Econ Geol 64:599-612

Hendricks SB (1937) The crystal structure of alunite and the jarosites. Am Mineral 22: 773-784

Herold H (1987) Zur Kristallchimie und Thermodynamik der Phosphate und Arsenate vom CrandalliteTyp. Thesis, University of Erlangen, Nürnberg, Germany

Hochella NIF Jr, Moore IN, Golla U, Putnis AA (1999) TEM study of samples from acid mine drainage systems: Metal-mineral association with implications for transport. Geochim Cosmochim Acta 63:3395-3406

Hofstra AH, LW, Rye RO, Folger HW, Phinisey JD, Loranger RJ, Dahl AR, Naeser CW, Stein HJ, Lewchuk L (1999) Age constraints on Jerritt Canyon and other Carlin-type gold deposits in the western United States: Relationship to mid-Tertiary extension and magmatism. Econ Geol 94:769-802

Ilchik RP (1990) Geology and geochemistry of the Vantage gold deposits, Alligator Ridge-Bald Mountain mining district, Nevada. Econ Geol 85:50-75

Itaya T, Arribas A Jr, Okada T (1996) Argon release systematics of hypogene and supergene alunite based on progressive heating experiments from 100 to 1000°C. Geochim Cosmochim Acta 60:4525-2535.

Jambor JL (1999) Nomenclature of the alunite supergroup. Can Mineral 37:1323-1341

Jirkovsky (1927) Casopis Narod Musea Praha 101:151 (in Palache et al. 1951)

John DA, Thomason RE, McKee EH (1989) Geology and K-Ar geochronology of the Paradise Peak mine and relationship of pre-Basin and Range extension to early Miocene precious metal mineralization in west-central Nevada. Econ Geol 84:631-649

John DA, Nash JT, Clark CW, Wulftange WH (1991) Geology, hydrothermal alteration, and mineralization at the Paradise Peak gold-silver-mercury deposit, Nye County, Nevada. *In* Raines GL, Lisle RE, Schafer RW, Wilkinson WH (eds) Geology and Ore Deposits of the Great Basin. Symp Procgs, Geol Soc Nevada (Reno) 2:1020-1050

Kashkai MA (1969) Alunite group and its structural analogs. Zapiski Vses Mineral Obshch 98:150-165 (in Russian)

Kashkai MA, Borovskaya TB, Babazade MA (1975) Determination of $\Delta G°_{f,298}$ of synthetic jarosite and its sulfate analogues. Geokhim 7:771-783 (in Russian)

Kato T, Miúra Y (1977) The crystal structures of jarosite and svanbergite. Mineral J (Japan) 8:419-430

Kelley KK (1960) Contributions to the data on theoretical metallurgy: XIII. High temperature heat content, heat capacity and entropy data for the elements and inorganic compounds. US Bur Mines Bull 584

Kelley KK, Shomate CH, Young FE, Naylor BF, Salo AE, Juffman EH (1946) Thermodynamic properties of ammonium and potassium alums and related substances with reference to extraction of alumina from clay and alunite. US Bur Mines Tech Paper 688

Khalaf FI (1990) Diagenetic alunite in clastic sequences, Kuwait, Arabian Gulf. Sedimentol 37:155-164

Kubisz J (1964) A study of minerals of the alunite-jarosite group. Polska Akad Nauk Prace Geol 22:1-90

Kubisz J (1970) Studies on synthetic alkali-hydronium jarosite: I. Synthesis of jarosite and natrojarosite. Mineral Polon 1:47-59

Langmuir D (1971) Particle size effect on the reaction goethite = hematite + water. Am J Sci 271:147-156

Lombardi G, Barbieri M (1983) The Tolfa Volcanics (Italy) alunitization process in the light of new chemical and Sr isotope data. Abstracts with Programs, Geol Soc Am 15:630

Mahin RA (1990) The mineralogy and geochemistry of the Apex germanium-gallium mine, southwestern Utah. MSc thesis, University of Utah, Salt Lake City, Utah

Menhert HH, Lipman PW, Steven TA (1973) Age of mineralization at Summitville, Colorado, as indicated by K-Ar dating of alunite. Econ Geol 68:399-412

Menchetti S, Sabelli C (1976) Crystal chemistry of the alunite series: crystal structure refinement of alunite and synthetic jarosite. N Jahrb Mineral Monatsh 406-417

Meyer C, Hemley JJ (1967) Wall rock alteration. *In* Barnes HL (ed) Geochemistry of Hydrothermal Ore Deposits. Holt, Rinehart, and Winston, New York, p 166-235

Meyer R, Peña dos Reis RB (1985) Paleosols and alunite silcretes in continental Cenozoic of western Portugal. J Sed Petrol 55:76-85

Nordstrom DK, Alpers CN (1999) Geochemistry of acid mine waters. *In* Plumlee GS, Logsdon MJ (eds) The Environmental Geochemistry of Mineral Deposits: Part A. Processes, Methods, and Health Issues. Rev Econ Geol 6A:133-160

Okada K, Hirabayashi J, Ossaka J (1982) Crystal structure of natroalunite and crystal chemistry of the alunite group. N Jahrb Mineral Monatsh 534-540

Ojeda JM (1986) Escondida porphyry copper deposit, II Region, Chile: Exploration drilling and current geological interpretation. *In* Papers, Mining Latin Am Conf, Santiago, Chile, 17-19 November 1986, Institution of Mining and Metallurgy, London UK, p 299-318

Palache C, Berman H, Frondel C (1951) The System of Mineralogy, Vol 2. John Wiley & Sons, New York
Parker RL (1962) Isomorphous substitution in natural and synthetic alunite. Am Mineral 47:127-136
Pécksay Z, Balogh K, Széky-Fux V, Gyarmati P (1986) Geochronological investigations on the Neogene volcanism of the Tokaj Mountains. Geol Carpathica 37:635-655
Perello, JA (1994) Geology, porphyry Cu-Au, and epithermal Cu-Au-Ag mineralization of the Tombulilato district, North Sulawesi, Indonesia. J Geochem Explor 50:221-256
Plummer LN, Parkhurst DL, Fleming GW, Dunkle SA (1988) A computer program incorporating Pitzer's equations for calculation of geochemical reactions in brines. US Geol Survey Water-Resources Invest Rept 88-4153
Polyak VJ, McIntosh WC, Guven N, Provencio P (1998) Age and origin of Carlsbad Cavern and related caves from $^{40}Ar/^{39}Ar$ of alunite. Science 279:1919-1922
Posnjak E, Merwin HE (1922) The system Fe_2O_3–SO_3–H_2O J Am Chem Soc 44:1965-1994
Powell R (1974) A comparison of some mixing models for crystalline silicate solutions. Contrib Mineral Petrol 46:265-274
Raymahashay BC (1969) A geochemical study of rock alteration by hot springs in the Paint Pot Hill area, Yellowstone Park. Geochim Cosmochim Acta 32:499-522
Richards JP, Noble SR, Pringle MS (1999) A revised Late Eocene age for porphyry Cu magmatism in the Escondida area, northern Chile. Econ Geol 94:1231-1247
Ripmeester JA, Ratcliffe CI, Dutrizac JE, Jambor JL (1986) Hydronium ion in the alunite-jarosite group. Can Mineral 24:435-447
Ripp GS, Kanakin SV (1998) Phosphate minerals in the metamorphosed high-alumina rocks of the Ichetui occurrence, Transbaikal region. Dokl Earth Sci 359:233-235
Ripp GS, Kanakin SV, Shcherbakova MN (1998) Phosphate mineralization in metamorphosed high-alumina rocks of the Ichetuyskoye ore occurrence. Zapiski Vseross Mineral Obshch 127(6):98-108 (in Russian)
Rye RO, Alpers, CN (1997) The stable isotope geochemistry of jarosite. US Geol Survey Open-File Rept 97-88
Rye RO, Bethke PM, Wasserman MD (1992) The stable isotope geochemistry of acid-sulfate alteration. Econ Geol 87:240-262
Rye RO, Bethke PM, Lanphere MA, Steven TA (2000) Neogene geomorphic and climatic evolution of the central San Juan Mountains, Colorado: K/Ar age and stable isotope data on supergene alunite and jarosite from the Creede mineral district. *In* Bethke PM, Hay RL (eds) Ancient Lake Creede: Its volcano-tectonic setting, history of sedimentation, and relation to mineralization in the Creede Mining District, Colorado. Geol Soc Am Spec Paper 346:95-104
Sander MV (1988) Geologic setting and the relation of epithermal gold-silver mineralization to wall rock alteration at the Round Mountain mine, Nye County, Nevada. *In* Schafer RW, Cooper JJ, Vikre PG (eds) Bulk mineable precious metal deposits of the western United States. Symposium proceedings, Geol Soc Nevada, Reno, p 375-416
Schmetzer K, Ottemann J, Bank H (1980) Schlossmacherite, $(H_3O,Ca)Al_3[(OH)_6 \mid ((S,As)\ O_4)_2]$, ein neues Mineral der Alunit–Jarosit–Riehe. N Jahrb Mineral Monatsh 215-222
Schoch AE, Beukes GJ, van der Westhuizen WA, de Bruiyn H (1989) Natroalunite from Koenabib, Pofadder District, South Africa. S Afr Tydskr Geol 92:20-28
Schwab RG, Götz C, Herold H, Pinto de Oliveira N (1993) Compounds of the crandallite type: Thermodynamic properties of Ca-, Sr-, Ba-, Pb-, La, Ce- to Gd- phosphates and –arsenates. N Jahrb Mineral Monatsh 551-568
Scott KM (1987) Solid solution in, and classification of, gossan-derived members of the alunite-jarosite family, northwest Queensland, Australia. Am Mineral 72:178-187
Shanin LL, Ivanov IB, Shipulin FK (1968) The possible use of alunite in K-Ar geochronometry. Geokhim 1:109-111
Silberman ML, Ashley RP (1970) Age of ore deposition at Goldfield, Nevada, from potassium-argon dating of alunite. Econ Geol 65:352-254
Sillitoe, RH, Bonham, HF Jr (1990) Sediment-hosted gold deposits: Distal products of magmatic-hydrothermal systems. Geology 18:157-161
Sillitoe, RH, Lorson RC (1994) Epithermal gold-silver-mercury deposits at Paradise Peak, Nevada: Ore controls, porphyry gold association, detachment faulting, and supergene oxidation. Econ Geol 89:1228-1248
Sillitoe RH, McKee EH (1996) Age of supergene oxidation and enrichment in the Chilean porphyry copper province. Econ Geol 91:164-179
Sillitoe RH, McKee EH, Vila T (1991) Reconnaissance K-Ar geochronology of the Maricunga gold-silver belt, northern Chile. Econ Geol 86:1261-1270

Steven TA, Cunningham CG, Naeser CW, Menhert HH (1979) Revised stratigraphy and radiometric ages of volcanic rocks and mineral deposits in the Marysvale area, west-central Utah. US Geol Survey Bull 1469

Stoffregen RE (1987) Genesis of acid-sulfate alteration and Au-Cu-Ag mineralization at Summitville, Colorado. Econ Geol 82:1575-1591

Stoffregen RE (1990) An experimental study of Na-K exchange between alunite and aqueous sulfate solutions. Am Mineral 75:209-220

Stoffregen RE (1993) Stability relations of jarosite and natrojarosite. Geochim Cosmochim Acta 57:2417-2419

Stoffregen RE, Alpers CN (1987) Woodhouseite and svanbergite in hydrothermal ore deposits: products of apatite destruction during advanced argillic alteration. Can Mineral 25:201-211

Stoffregen RE, Alpers CN (1992) Observations on the unit cell parameters, water contents and δD of natural and synthetic alunites. Am Mineral 77:1092-1098

Stoffregen RE, Cygan GL (1990) An experimental study of Na-K exchange between alunite and aqueous sulfate solutions. Am Mineral 75:209-220

Stoffregen RE, Rye RO, Wasserman MD (1994) Experimental studies of alunite: II. ^{18}O–^{16}O and D–H fractionation factors between alunite and water at 250-450 °C. Geochim Cosmochim Acta 58:903-916

Szymanski JT (1985) The crystal structure of plumbojarosite $Pb[Fe_3SO_4)_2(OH)_6]_2$. Can Mineral 23:659-668

Teal L, Branham A (1997) Geology of the Mike gold-copper deposit, Eureka County, Nevada. Soc Econ Geol Guidebook Series 28:257-276

Tingley JV, Berger BR (1985) Lode gold deposits of Round Mountain, Nevada. Nevada Bur Mines Geol Bull 100

Tozawa K, Sasaki K, Umetsu Y (1983) The effect of the second dissociation of sulfuric acid on hydrometallurgical processes: The electrical conductivity of sulfuric acid-containing electrolytes and the hydrolysis of ferric sulfate solutions at elevated temperatures. *In* Osseo-Asare K, Miller JD (Eds) Hydrometallurgy Research, Development and Practice. TMS-AIME, New York, p 375-389

Umetsu Y, Tozzawa K, Sasaki K (1977) The hydrolysis of ferric sulfate solutions at elevated temperatures. Can Metall Quart 16:111-117

Vasconcelos PM, Brimhall GH, Becker TA, Renne PR (1994) $^{40}Ar/^{39}Ar$ analysis of supergene jarosite and alunite: Implications to the paleoweathering history of the western USA and West Africa. Geochim Cosmochim Acta 58:401-420

Vasconcelos PM (1999a) K–Ar and $^{40}Ar/^{39}Ar$ geochronology of weathering processes. Ann Rev Earth Planet Sci 27:183-229

Vasconcelos PM (1999b) $^{40}Ar/^{39}Ar$ geochronology of supergene processes in ore deposits. *In* Lambert DD, Ruiz J (eds) Application of Radiogenic Isotopes to Ore Deposit Research and Exploration. Rev Econ Geol 12:73-113

Wang R, Bradley WF, Steinfink H (1965) The crystal structure of alunite. Acta Crystallogr 18:249-252

Webb AW, McDougall I (1968) The geochronology of the igneous rocks of eastern Queensland. J Geol Soc Aust 15:313-343

Whalen JB, Britten RM, McDougall I (1982) Geochronology and geochemistry of the Freida River prospect area, Papua New Guinea. Econ Geol 77:592-616

Williams CL (1992) Breccia bodies in the Carlin trend, Elko and Eureka counties, Nevada: Classification, interpretation, and roles in ore formation. MSc thesis, Colorado State University, Fort Collins, Colorado

Wise WS (1975) Solid solution between the alunite, woodhouseite, and crandallite mineral series. N Jahrb Mineral Monatsh 540-545

Zotov AV (1967) Recent formation of alunite in the Kipyashcheye ("boiling") crater lake, Golovnin volcano, Kunashir Island. Dokl Akad Nauk SSSR 174:124-127 (in Russian)

Zotov AV, Mironova GD, Rusinov VL (1973) Determination of $\Delta G_{f,298}$ of jarosite synthesized from a natural solution. Geokhim 5:739-745 (in Russian)